A methodology for the estimation of the effective yield function of isotropic composites

I Papadioti, Kostas Danas, N. Aravas

A METHODOLOGY FOR THE ESTIMATION OF THE EFFECTIVE YIELD FUNCTION OF ISOTROPIC COMPOSITES

I. Papadioti[1,2], **K. Danas**[3] and **N. Aravas**[1,4*]

[1] Department of Mechanical Engineering
University of Thessaly
38334 Volos
GREECE

[2] Institute for Research and Technology Thessaly (I.RE.TE.TH.)
Center for Research and Technology - Hellas
38333 Volos
GREECE

[3] Laboratoire de Mécanique des Solides,
C.N.R.S., École Polytechnique, University of Paris-Saclay,
Palaiseau, FRANCE

[4] International Institute for Carbon Neutral Energy Research (WPI-I2CNER)
Kyushu University,
744 Moto-oka, Nishi-ku, Fukuoka 819-0395
JAPAN

Abstract

In this work we derive a general model for $N-$phase isotropic, incompressible, rate-independent elasto-plastic materials at finite strains. The model is based on the nonlinear homogenization variational (or modified secant) method which makes use of a linear comparison composite (LCC) material to estimate the effective flow stress of the nonlinear composite material. The homogenization approach leads to an optimization problem which needs to be solved numerically for the general case of a $N-$phase composite. In the special case of a two-phase composite an analytical result is obtained for the effective flow stress of the elasto-plastic composite material. Next, the model is validated by periodic three-dimensional unit cell calculations comprising a large number of spherical inclusions (of various sizes and of two different types) distributed randomly

in a matrix phase. We find that the use of the lower Hashin-Shtrikman bound for the LCC gives the best predictions by comparison with the unit cell calculations for both the macroscopic stress-strain response as well as for the average strains in each of the phases. The formulation is subsequently extended to include hardening of the different phases. Interestingly, the model is found to be in excellent agreement even in the case where each of the phases follows a rather different hardening response.

Keywords: Homogenization; Elasto-plasticity; Composite materials; Finite strains

* Corresponding author. Fax: +30 2421 074009.
E-mail addresses: aravas@uth.gr (N. Aravas), kdanas@lms.polytechnique.fr (K. Danas).

1 Introduction

The present work deals with the analytical and numerical estimation of the effective as well as the phase average response of $N-$phase incompressible isotropic elasto-plastic metallic composites. Special attention is given to particulate microstructures, i.e., composite materials which can be considered to comprise a distinct matrix phase and an isotropic distribution of spherical particles [46] (or in a more general setting an isotropic distribution of phases [45]). In the present study, the particles are considered to be stiffer than the matrix phase, which is the case in most metallic materials of interest, such as TRIP steels, dual phase steels, aluminum alloys and others. Such materials, usually contain second-phase particles (e.g., intermetallics, carbon particles) or just second and third phase variants (e.g., retained austenite, bainite, martensitic phases). In addition, these phases/particles tend to reinforce the yield strength of the composite while they usually have different strength and hardening behavior than the host matrix phase.

In the literature of nonlinear homogenization there exists a large number of studies for two-phase composite materials. The reader is referred to Ponte Castañeda and Suquet [33], Ponte Castañeda [32], Idiart *et al.* [15], and Idiart [16] for a review of the nonlinear homogenization schemes such as the ones used in the present work and relevant estimates. Nonetheless, very few studies exist in the context of three- or $N-$phase rate independent elasto plastic composites.

In view of this, the present work uses the nonlinear variational homogenization method (Ponte Castañeda [29]) or equivalently the modified secant method (Suquet [43]), which makes use of a linear comparison composite (LCC) material, to estimate the effective response of a $N-$phase nonlinear composite material. Even though, this method exists for several years most of the studies in the context of composite materials have been focused on two-phase composites where the optimization process required by the method can be done analytically (see for instance [8]). Nevertheless, as the number of phases increases to three or more the optimization can only be done numerically. Perhaps, that is the reason that in his original work, Ponte Castañeda [30] proposed general expressions (and bounds) for $N-$phase composites, but its numerical/analytical resolution remained untractable until today due to the complex optimization procedures required by the nonlinear homogenization method.

It should be pointed out at this point that these homogenization theories treat separately the elastic (which in the present case is trivial) and the plastic homogenization problem. That of course has certain impact if cyclic loading is considered which is beyond the scope of the present work and is not considered here. Nevertheless, recently, Lahellec and Suquet [19] proposed an incremental variational formulation for materials with a hereditary behavior described by two potentials: a free energy and a dissipation function. This method has been introduced mainly to deal with the coupled elasto-plastic response of composites in an attempt to resolve the cyclic response of these materials (see also recent work by Brassart *et al.* [5]). Note that these more advanced methods use the aforementioned or variants of the LCC estimates. In this regard, the present study, albeit not using this coupled scheme, reveals the nature of equations required to deal with a general $N-$phase composite material and could be potentially useful in the future for such more complete incremental schemes, which are based upon those simpler LCC homogenization theories.

1.1 Scope of the present work and major results

The scope of the present work is to provide a semi-analytical model for $N-$phase isotropic, incompressible rate-independent elasto-plastic materials. Simple analytical expressions are given for the effective yield stress of a two-phase composite (see also [8]), while a simple semi-analytical expression (requiring the solution of a constrained optimization problem for $N-1$ scalar quantities) is given for the $N-$phase composite. Additional analytical expresssions are also provided for the phase concentration tensors and average strains in each phase in terms of the aforementioned optimized scalar quantities. In the context of two- and three-phase materials the model is assessed by appropriate three-dimensional multi-particle two- and three-phase periodic unit cell calculations considering both hardening and non-hardening phases. The agreement is found to be good not only for the effective yield stress but also for the phase average strains thus allowing for the extension of this model to include arbitrary isotropic hardening of the phases.

Specifically, we use the methodology developed by Ponte Castañeda and co-workers [29, 43] to derive a model for the rate-independent elastoplastic behavior of a macroscopically isotropic composite comprising N phases. When the constituent phases are perfectly plastic the corresponding flow stress of the composite material $\tilde{\sigma}_0$ is determined from the solution of a constrained optimization problem:

$$\tilde{\sigma}_0 = \sqrt{\inf_{\substack{y^{(i)}\geq 0 \\ y^{(1)}=1 \\ i=2,\ldots,N}} \left(\sum_{r=1}^{N} c^{(r)} {\sigma_0^{(r)}}^2 \, y^{(r)}\right) \left(\sum_{p=1}^{N} \frac{c^{(p)}}{3\,y^{(p)}+2\,y_0}\right) \left(\sum_{s=1}^{N} \frac{c^{(s)}\,y^{(s)}}{3\,y^{(s)}+2\,y_0}\right)^{-1}} \,. \qquad (1)$$

where N is the number of phases, $(c^{(i)}, \sigma_0^{(i)})$ are the volume fraction and flow stress of phase i, and $y^{(i)}$ are positive optimization parameters. In turn, y_0 is a reference scalar to be chosen according to various linear homogenization schemes. For instance, best results are obtained with the well known Hashin-Shtrikman lower bound choice, i.e., $y_0 = y^{(1)} = 1$.
In the special case of a two-phase composite ($N = 2$), the optimization problem is solved analytically and the estimate for the composite flow stress becomes

$$\frac{\tilde{\sigma}_0}{\sigma_0^{(1)}} = \begin{cases} \frac{5\,c^{(2)}\,r + c^{(1)}\sqrt{9+6\,c^{(2)}-6\,c^{(2)}\,r^2}}{3+2\,c^{(2)}} & \text{if} \quad 1 \leq r \leq 5/\sqrt{4+6\,c^{(2)}}, \\ \frac{1}{2}\sqrt{4+6\,c^{(2)}} & \text{if} \quad r \geq 5/\sqrt{4+6\,c^{(2)}}, \end{cases} \qquad (2)$$

where $r = \sigma_0^{(2)}/\sigma_0^{(1)}$ is the contrast ratio. The predictions of the homogenization model agree well with the predictions of detailed three-dimensional unit cell finite element calculations as shown in the following.
The homogenization technique provides also accurate estimates for the average strains in the constituent phases. These estimates form the basis for the development of an approximate analytical model for the elastoplastic behavior of a composite with hardening phases. A method for the numerical integration of the resulting elastic-plastic equations is developed and the model is implemented into the ABAQUS general purpose finite element code. The predictions of the model agree well with the results of detailed unit cell finite element calculations of a composite with hardening phases.
Standard notation is used throughout. Boldface symbols denote tensors the orders of which are indicated by the context. The usual summation convention is used for repeated Latin indices of tensor components with respect to a fixed Cartesian coordinate system with base

vectors $\mathbf{e}_i$ $(i = 1, 2, 3)$. The prefice det indicates the determinant, a superscript T indicates the transpose, and the subscripts s and a the symmetric and anti-symmetric parts of a second-order tensor. A superposed dot denotes the material time derivative. Let $\mathbf{A}$, $\mathbf{B}$ be second-order tensors, and $\mathbf{C}$, $\mathbf{D}$ fourth-order tensors; the following products are used in the text: $(\mathbf{A}\cdot\mathbf{B})_{ij} = A_{ik}\,B_{kj}$, $\mathbf{A}:\mathbf{B} = A_{ij}\,B_{ij}$, $(\mathbf{A}\,\mathbf{B})_{ijkl} = A_{ij}\,B_{kl}$, $(\mathbf{C}:\mathbf{A})_{ij} = C_{ijkl}\,A_{kl}$, and $(\mathbf{C}:\mathbf{D})_{ijkl} = C_{ijpq}\,D_{pqkl}$. The inverse $\mathbf{C}^{-1}$ of a fourth-order tensor $\mathbf{C}$ that has the "minor" symmetries $C_{ijkl} = C_{jikl} = C_{ijlk}$ is defined so that $\mathbf{C}:\mathbf{C}^{-1} = \mathbf{C}^{-1}:\mathbf{C} = \boldsymbol{\mathcal{I}}$, where $\boldsymbol{\mathcal{I}}$ is the symmetric fourth-order identity tensor with Cartesian components $\mathcal{I}_{ijkl} = (\delta_{ik}\,\delta_{jl}+\delta_{il}\,\delta_{jk})/2$, δ_{ij} being the Kronecker delta.

2 Power-law creep and perfect plasticity

We consider an incompressible creeping solid characterized by a power-law stress potential U of the form

$$U\,(\sigma_e) = \frac{\sigma_0\,\dot{\varepsilon}_0}{n+1}\,\left(\frac{\sigma_e}{\sigma_0}\right)^{n+1}, \tag{3}$$

where σ_0 is a reference stress, $\dot{\varepsilon}_0$ a reference strain rate, n the creep exponent $(1 \le n \le \infty)$, $\sigma_e = \sqrt{\frac{3}{2}\,\mathbf{s}:\mathbf{s}}$ the von Mises equivalent stress, $\boldsymbol{\sigma}$ the stress tensor, $p = \sigma_{kk}/3$ the hydrostatic stress, and $\mathbf{s} = \boldsymbol{\sigma} - p\,\boldsymbol{\delta}$ the stress deviator, $\boldsymbol{\delta}$ being the second-order identity tensor. The corresponding deformation rate $\mathbf{D}$ is defined as

$$\mathbf{D} = \frac{\partial U}{\partial \boldsymbol{\sigma}} = \dot{\bar{\varepsilon}}\,\mathbf{N}, \qquad \dot{\bar{\varepsilon}} = \dot{\varepsilon}_0\left(\frac{\sigma_e}{\sigma_0}\right)^n, \qquad \mathbf{N} = \frac{\partial \sigma_e}{\partial \boldsymbol{\sigma}} = \frac{3}{2\,\sigma_e}\mathbf{s}\,, \tag{4}$$

where $\mathbf{N}$ is a second order tensor of constant magnitude $(\mathbf{N}:\mathbf{N} = \frac{3}{2})$ that defines the direction of $\mathbf{D}$ and $\dot{\bar{\varepsilon}} = \sqrt{\frac{2}{3}\,\mathbf{D}:\mathbf{D}}$ is the equivalent plastic strain rate that defines the magnitude of $\mathbf{D}$. Note that $D_{kk} = 0$.

The special case in which the exponent takes the value of unity $(n = 1)$ corresponds to a linearly viscous solid:

$$U_L(\sigma_e) = \frac{\sigma_e^2}{6\,\mu}, \qquad \mathbf{D} = \frac{\partial U_L}{\partial \boldsymbol{\sigma}} = \frac{\mathbf{s}}{2\,\mu}, \tag{5}$$

where $\mu = \sigma_0/(3\,\dot{\varepsilon}_0)$ is the viscosity.

The other limiting case $n \to \infty$ corresponds to a perfectly plastic solid that obeys the von Mises yield condition with flow stress σ_0. In this case the stress function (3) becomes[1]

$$U_\infty(\sigma_e) = \begin{cases} 0 & \text{when} \quad \sigma_e \le \sigma_0\,, \\ \infty & \text{when} \quad \sigma_e > \sigma_0\,. \end{cases} \tag{6}$$

The threshold stress σ_0 in (6) is the flow stress of the material, and the flow rule is written in the form

$$\mathbf{D} = \dot{\bar{\varepsilon}}\,\mathbf{N}, \qquad \mathbf{N} = \frac{3}{2\,\sigma_e}\mathbf{s}\,, \qquad (\text{with} \quad \dot{\bar{\varepsilon}} = 0 \quad \text{if} \quad \sigma_e < \sigma_0), \tag{7}$$

where the equivalent plastic strain rate $\dot{\bar{\varepsilon}}$ is not defined locally by the constitutive equations and becomes one of the primary unknowns in the rate boundary value problem.

[1] Here we take into account that $\lim_{n\to\infty} \frac{A^{n+1}}{n+1} = \begin{cases} 0 & \text{if } A \le 1, \\ \infty & \text{if } A > 1. \end{cases}$

3 The homogenization method

We consider a composite material made of N isotropic, incompressible viscoplastic phases. The phases are distributed randomly and isotropically and are characterized by viscoplastic stress potentials $U^{(r)}$ of the form (3) with constants $\left(\sigma_0^{(r)}, \dot{\varepsilon}_0, n^{(r)}\right)$ and $\mu^{(r)}$ in the linear case, i.e.,

$$U^{(r)}\left(\sigma_e^{(r)}\right) = \frac{\sigma_0^{(r)}\,\dot{\varepsilon}_0}{n^{(r)}+1}\left(\frac{\sigma_e^{(r)}}{\sigma_0^{(r)}}\right)^{n^{(r)}+1}, \qquad U_L^{(r)}(\sigma_e^{(r)}) = \frac{{\sigma_e^{(r)}}^2}{6\,\mu^{(r)}}, \tag{8}$$

where $\sigma_e^{(r)}$ is the von Mises equivalent stress in phase r. The volume fraction of each phase is $c^{(r)}$ $\left(\sum_{r=1}^{N} c^{(r)} = 1\right)$.
The constitutive equation of the isotropic nonlinear composite is written in terms of the effective viscoplastic stress potential $\tilde{U}(\boldsymbol{\sigma})$, so that

$$\mathbf{D} = \frac{\partial \tilde{U}}{\partial \boldsymbol{\sigma}}, \tag{9}$$

where $\boldsymbol{\sigma}$ and $\mathbf{D}$ are respectively the macroscopic stress and deformation rate in the composite. An estimate for $\tilde{U}$ is obtained by using the variational methodology of Ponte Castañeda and co-workers ([29], [31], [33]). This methodology has also been proposed independently for power-law materials by Michel and Suquet [25] and interpreted as a secant homogenization method by Suquet [43]. The final form of the estimate reads (Ponte Castañeda [30])

$$\tilde{U}(\sigma_e) = \sup_{\mu^{(r)}\geq 0}\left[\tilde{U}_L\left(\sigma_e, \tilde{\mu}(\mu^{(r)})\right) - \sum_{r=1}^{N} c^{(r)}\, v^{(r)}\left(\mu^{(r)}\right)\right], \qquad \tilde{U}_L = \frac{\sigma_e^2}{6\,\tilde{\mu}(\mu^{(r)})}, \tag{10}$$

where σ_e is the macroscopic von Mises equivalent stress,

$$v^{(r)}\left(\mu^{(r)}\right) = \sup_{\sigma_e^{(r)}\geq 0}\left[U_L^{(r)}\left(\sigma_e^{(r)}, \mu^{(r)}\right) - U^{(r)}\left(\sigma_e^{(r)}\right)\right], \tag{11}$$

$$U_L^{(r)} = \frac{{\sigma_e^{(r)}}^2}{6\,\mu^{(r)}}, \qquad U^{(r)} = \frac{\sigma_0^{(r)}\,\dot{\varepsilon}_0}{n^{(r)}+1}\left(\frac{\sigma_e^{(r)}}{\sigma_0^{(r)}}\right)^{n^{(r)}+1}. \tag{12}$$

The effective stress potential $\tilde{U}(\boldsymbol{\sigma})$ is defined in (10) in terms of the quadratic effective stress potential $\tilde{U}_L$ of a "linear comparison composite" (LCC) evaluated at the macroscopic stress σ_e and the "corrector functions" $v^{(r)}$, which are defined in (11) as the optimal difference between the quadratic potentials $U_L^{(r)}$ and the actual potentials of the non-linear materials $U^{(r)}$. The stress tensors $\sigma_e^{(r)}$ in (11) are obtained by the "sup" operation in that equation and hence $v^{(r)}$ are only functions of the individual viscosities of the linearized phases, $\mu^{(r)}$. It is worth noting at this point that the estimate (10) of $\tilde{U}$ may have the character of a rigorous bound provided that the corresponding estimate $\tilde{U}_L$ has also the same character of a bound as discussed in the following. Nonetheless the scope of the present work is to insist mainly on a good estimate by comparison with numerical unit cell calculations and not necessarily on rigorous bounds.
In this view, the quadratic potential $\tilde{U}_L$ of the LCC in (10b) uses the effective viscosity $\tilde{\mu}$ of the LCC that depends on the individual viscosities $\mu^{(r)}$ and the corresponding volume

fractions $c^{(r)}$. One way to estimate $\tilde{\mu}$ is to use the well-known Hashin-Shtrikman relationship for particulate composites (e.g., see Willis [46])

$$\tilde{\mu}\left(\mu^{(r)}\right) = \left(\sum_{s=1}^{N} \frac{c^{(s)}\,\mu^{(s)}}{3\,\mu_0 + 2\,\mu^{(s)}}\right)\left(\sum_{r=1}^{N} \frac{c^{(r)}}{3\,\mu_0 + 2\,\mu^{(r)}}\right)^{-1}, \tag{13}$$

where μ_0 is a "reference viscosity" to be chosen appropriately. An upper bound for $\tilde{\mu}$ is produced by (13) when μ_0 is chosen to be the maximum of all $\mu^{(r)}$ and a lower bound is produced when μ_0 is the minimum of all $\mu^{(r)}$ (Willis [46]).
An important observation made by several authors is that the Hashin-Shtrikman *bounds* are accurate *estimates* for composites with particulate microstructures, at least for two-phase systems at moderate volume fraction (Bonnenfant *et al.* [3]); in particular, the upper bound is a good estimate when the stiffest material is the matrix phase and contains inclusions of the most compliant material, whereas the lower bound is a good estimate for the inverse situation in which the most compliant material is the matrix phase containing inclusions of the stiffest material.
When no phase plays clearly the role of a matrix, the effective properties of the composite may be estimated by the self-consistent method of Hill [14]. In this case, the relevant microstructure is granular in character, being composed of ellipsoidal particles of the different phases with varying size so as to fill space. Equation (13) provides Hill's self-consistent estimate, if μ_0 is identified with the effective modulus $\tilde{\mu}$; in this case, (13) becomes a polynomial equation of order $2\,N$ for $\tilde{\mu}$ (Willis [46]).

3.1 Strain-rate concentration in the phases

An approximation for the strain field in the non-linear composite may be obtained from the strain field in the LCC evaluated at the optimal comparison moduli $\hat{\mu}^{(r)}$ defined by the optimization problem in (10). In particular, the *average* deformation rate field in the phases $\mathbf{D}^{(r)}$ may be written in terms of the macroscopic deformation rate $\mathbf{D}$ in the form (Ponte Castañeda and co-workers [31], [37], [17],[34]):

$$\mathbf{D}^{(r)} = \mathbf{A}^{(r)}\left(\hat{\mu}^{(i)}(\sigma_e)\right) : \mathbf{D}, \qquad r = 1, 2, \cdots, N, \tag{14}$$

where $\mathbf{A}^{(r)}$ are the fourth-order strain concentration tensors of the LCC, evaluated at the *optimal* values[2], $\hat{\mu}^{(r)}$, of the comparison moduli, defined by the solution of the optimization problem in (10). It is emphasized that the optimal values $\hat{\mu}^{(r)}$ depend in a nonlinear manner upon the macroscopic von Mises equivalent σ_e, and consequently the strain concentration tensors $\mathbf{A}^{(r)}$ are in general nonlinear functions of the macroscopic stress tensor $\boldsymbol{\sigma}$.
For isotropic composite materials with random microstructures and "ellipsoidal symmetry", $\mathbf{A}^{(r)}$ is of the form (Ponte Castañeda [31])

$$\mathbf{A}^{(r)} = \mathbf{E}^{(r)} : \left(\sum_{s=1}^{N} c^{(s)}\,\mathbf{E}^{(s)}\right)^{-1}, \qquad \mathbf{E}^{(r)} = \left[\boldsymbol{\mathcal{I}} + \mathbf{S}_0 : \boldsymbol{\mathcal{L}}_0^{-1} : \left(\boldsymbol{\mathcal{L}}^{(r)} - \boldsymbol{\mathcal{L}}_0\right)\right]^{-1}, \tag{15}$$

[2]Henceforth the superscript $(\hat{\cdot})$ serves to denote the optimal value of the relevant quantity obtained by the corresponding optimization described in the previous section.

where $\boldsymbol{\mathcal{I}}$ is the symmetric fourth order identity tensor with Cartesian components $\mathcal{I}_{ijkl} = (\delta_{ik}\,\delta_{jl}+\delta_{il}\,\delta_{jk})/2$, $\mathbf{S}_0$ is the well known tensor of Eshelby [9] for the linear "reference material" with elasticity tensor $\boldsymbol{\mathcal{L}}_0$ introduced in (13), and

$$\boldsymbol{\mathcal{L}}_0 = 2\,\mu_0\,\boldsymbol{\mathcal{K}} + 3\,\kappa_0\,\boldsymbol{\mathcal{J}}, \quad \boldsymbol{\mathcal{L}}^{(r)} = 2\,\hat{\mu}^{(r)}\,\boldsymbol{\mathcal{K}} + 3\,\kappa^{(r)}\,\boldsymbol{\mathcal{J}}, \quad \boldsymbol{\mathcal{J}} = \frac{1}{3}\boldsymbol{\delta}\,\boldsymbol{\delta}, \quad \boldsymbol{\mathcal{K}} = \boldsymbol{\mathcal{I}} - \boldsymbol{\mathcal{J}}. \tag{16}$$

The quantities (μ_0, κ_0) and $(\hat{\mu}^{(r)}, \kappa^{(r)})$ in (16) are the shear and bulk viscosities of the LCC; the bulk viscosities κ_0 and $\kappa^{(r)}$ are set to ∞ after the final expression for $\mathbf{D}^{(r)}$ in (14) is derived, in order to take into account the incompressible nature of the phases and the composite.

For composites consisting of an isotropic matrix and a uniform distribution of *spherical* inclusions, the Eshelby tensor has the form

$$\mathbf{S}_0 = \frac{6\,(\kappa_0 + 2\,\mu_0)}{5\,(3\,\kappa_0 + 4\,\mu_0)}\boldsymbol{\mathcal{K}} + \frac{3\,\kappa_0}{3\,\kappa_0 + 4\,\mu_0}\boldsymbol{\mathcal{J}}. \tag{17}$$

Using (16) and (17) in (15b) and taking into account that $\boldsymbol{\mathcal{J}} : \boldsymbol{\mathcal{J}} = \boldsymbol{\mathcal{J}}$, $\boldsymbol{\mathcal{K}} : \boldsymbol{\mathcal{K}} = \boldsymbol{\mathcal{K}}$, and $\boldsymbol{\mathcal{J}} : \boldsymbol{\mathcal{K}} = \mathbf{0}$, we conclude that

$$\mathbf{E}^{(r)} = \frac{5\,\mu_0\,(3\,\kappa_0 + 4\,\mu_0)}{\mu_0\,(9\,\kappa_0 + 8\,\mu_0) + 6\,(\kappa_0 + 2\,\mu_0)\,\hat{\mu}^{(r)}}\boldsymbol{\mathcal{K}} + \frac{3\,\kappa_0 + 4\,\mu_0}{3\,\kappa^{(r)} + 4\,\mu_0}\boldsymbol{\mathcal{J}}. \tag{18}$$

Then, using (15), after some lengthy but otherwise straightforward calculations we reach the following expression for the strain concentration tensors:

$$\mathbf{A}^{(r)} = \frac{1}{3\,\kappa^{(r)} + 4\,\mu_0}\left(\sum_{s=1}^{N}\frac{c^{(s)}}{3\,\kappa^{(s)} + 4\,\mu_0}\right)^{-1}\boldsymbol{\mathcal{J}} + \\ + \frac{1}{\mu_0\,(9\,\kappa_0 + 8\,\mu_0) + 6\,(\kappa_0 + 2\,\mu_0)\,\hat{\mu}^{(r)}}\left[\sum_{s=1}^{N}\frac{c^{(s)}}{\mu_0\,(9\,\kappa_0 + 8\,\mu_0) + 6\,(\kappa_0 + 2\,\mu_0)\,\hat{\mu}^{(s)}}\right]^{-1}\boldsymbol{\mathcal{K}}. \tag{19}$$

Finally, using (14), taking into account the incompressibility condition $D_{kk} = 0$ (or $\boldsymbol{\mathcal{J}} : \mathbf{D} = \mathbf{0}$), and considering the limit $\kappa_0 \to \infty$, we find

$$\mathbf{D}^{(r)} = \lim_{\kappa_0 \to \infty}\left(\mathbf{A}^{(r)} : \mathbf{D}\right) = \alpha^{(r)}\,\mathbf{D}, \qquad \boxed{\alpha^{(r)} = \frac{1}{3\,\mu_0 + 2\,\hat{\mu}^{(r)}}\left(\sum_{s=1}^{N}\frac{c^{(s)}}{3\,\mu_0 + 2\,\hat{\mu}^{(s)}}\right)^{-1}}. \tag{20}$$

We emphasize again that *the strain concentration factors $\alpha^{(r)}$ depend in general on the macroscopic stress $\boldsymbol{\sigma}$ (or macroscopic deformation rate $\mathbf{D}$) through the optimal moduli $\hat{\mu}^{(i)}$*. Equation (20) implies that

$$\dot{\bar{\varepsilon}}^{(r)} = \sqrt{\frac{2}{3}\,\mathbf{D}^{(r)} : \mathbf{D}^{(r)}} = \alpha^{(r)}\,\sqrt{\frac{2}{3}\,\mathbf{D} : \mathbf{D}} = \alpha^{(r)}\,\dot{\bar{\varepsilon}} \qquad \text{or} \qquad \boxed{\frac{d\bar{\varepsilon}^{(r)}}{d\bar{\varepsilon}} = \alpha^{(r)}}, \tag{21}$$

where $\dot{\bar{\varepsilon}}^{(r)}$ and $\dot{\bar{\varepsilon}}$ are the average equivalent strain rates in the phases and the average macroscopic equivalent strain rate respectively.

3.2 Perfectly plastic phases

We consider the case of perfectly plastic phases ($n^{(r)} \to \infty$). The optimization in (10) and (11) as $n^{(r)} \to \infty$ is carried out in three steps. In the first step, we consider the optimization over $\sigma_e^{(r)}$ in (11). All creep exponents are set equal in the second step, i.e., we set $n^{(1)} = n^{(2)} = \cdots = n^{(N)} \equiv n$. In the final third step we consider the limit $n \to \infty$. Details of the calculations are given in the following.

Step 1: Calculation of $\sigma_e^{(r)}$ in (11)
The "inner" optimization in (11) is carried out by setting equal to zero the derivatives

$$\frac{\partial}{\partial \sigma_e^{(r)}} \left(U_L^{(r)} - U^{(r)} \right) = 0, \tag{22}$$

which defines the optimal values of $\sigma_e^{(r)}$ as

$$\sigma_e^{(r)} = \left[\frac{\left(\sigma_0^{(r)}\right)^{n^{(r)}}}{3\,\mu^{(r)}\,\dot{\varepsilon}_0} \right]^{\frac{1}{n^{(r)}-1}} \equiv \hat{\sigma}_e^{(r)}. \tag{23}$$

When the optimal values $\hat{\sigma}_e^{(r)}$ are substituted into (10), the expression for the estimate of the effective stress potential becomes

$$\tilde{U}(\sigma_e) = \sup_{\mu^{(r)} \geq 0} \left\{ \frac{\sigma_e^2}{6\,\tilde{\mu}(\mu^{(r)})} - \frac{1}{2} \sum_{r=1}^{N} \frac{n^{(r)}-1}{n^{(r)}+1} \left[\frac{\left(\sigma_0^{(r)}\right)^{n^{(r)}}}{\dot{\varepsilon}_0} \right]^{\frac{2}{n^{(r)}-1}} \frac{c^{(r)}}{\left(3\,\mu^{(r)}\right)^{\frac{n^{(r)}+1}{n^{(r)}-1}}} \right\}, \tag{24}$$

where $\tilde{\mu}(\mu^{(r)})$ is defined in (13). Substitution of the expression (13) for $\tilde{\mu}$ into (24) leads to

$$\tilde{U}(\sigma_e) = \sup_{\substack{y^{(r)} \geq 0 \\ y^{(1)}=1}} \sup_{\mu^{(1)}>0} \left[F\left(y^{(r)}\right) \frac{\sigma_e^2}{6\,\mu^{(1)}} - I\left(\mu^{(1)}, y^{(r)}\right) \right], \tag{25}$$

where

$$F\left(y^{(r)}\right) = \frac{\mu^{(1)}}{\tilde{\mu}} = \left(\sum_{r=1}^{N} \frac{c^{(r)}\,y^{(r)}}{3\,y^{(r)} + 2\,y_0} \right) \left(\sum_{s=1}^{N} \frac{c^{(s)}}{3\,y^{(s)} + 2\,y_0} \right)^{-1}, \tag{26}$$

$$I\left(\mu^{(1)}, y^{(r)}\right) = \frac{1}{2} \sum_{r=1}^{N} c^{(r)} \frac{n^{(r)}-1}{n^{(r)}+1} \left[\frac{\left(\sigma_0^{(r)}\right)^{n^{(r)}}}{\dot{\varepsilon}_0} \right]^{\frac{2}{n^{(r)}-1}} \left(\frac{y^{(r)}}{3\,\mu^{(1)}} \right)^{\frac{n^{(r)}+1}{n^{(r)}-1}}, \tag{27}$$

$$y^{(r)} = \frac{\mu^{(1)}}{\mu^{(r)}} \quad (\text{with} \quad y^{(1)} = 1), \qquad \text{and} \qquad y_0 = \frac{\mu^{(1)}}{\mu_0}. \tag{28}$$

The optimal values of $y^{(r)}$ in (25) depend on the values of the volume fractions $c^{(r)}$, the material properties $(\sigma_0^{(r)}, n^{(r)}, \dot{\varepsilon}_0)$, and the macroscopic von Mises equivalent stress σ_e.

The strain concentration values $\alpha^{(r)}$ defined in (20) can be written in the form

$$\alpha^{(r)} = \frac{\hat{y}^{(r)}}{3\,\hat{y}^{(r)} + 2\,y_0} \left(\sum_{s=1}^{N} \frac{c^{(s)}\,\hat{y}^{(s)}}{3\,\hat{y}^{(s)} + 2\,y_0} \right)^{-1}, \quad r = 2, ..., N, \tag{29}$$

where $\hat{y}^{(r)}$ are the optimal values of $y^{(r)}$ resulting from the optimization in (25).

Step 2: Equal creep exponents $\left(n^{(1)} = n^{(2)} = \cdots = n^{(N)} \equiv n\right)$

When all "creep exponents" are set equal, i.e., $n^{(1)} = n^{(2)} = \cdots = n^{(N)} \equiv n$, equation (25) becomes

$$\tilde{U} = \sup_{\substack{y^{(r)} \geq 0 \\ y^{(1)} = 1}} \sup_{\mu^{(1)} > 0} \left[\frac{\sigma_e^2}{6\,\mu^{(1)}} F\left(y^{(r)}\right) - \frac{n-1}{2(n+1)} \frac{H\left(y^{(r)}\right)}{\left(3\,\mu^{(1)}\right)^{\frac{n+1}{n-1}}} \right], \tag{30}$$

where $F\left(y^{(r)}\right)$ is defined in (26) and

$$H\left(y^{(r)}\right) = \sum_{r=1}^{N} c^{(r)} \left[\frac{\left(\sigma_0^{(r)}\right)^n}{\dot{\varepsilon}_0} \right]^{\frac{2}{n-1}} \left(y^{(r)}\right)^{\frac{n+1}{n-1}}. \tag{31}$$

The optimal value of $\mu^{(1)}$ in (30) is determined by calculating the partial derivative of the quantity in brackets with respect to $\mu^{(1)}$ and setting it equal to zero. The resulting value for $\mu^{(1)}$ is

$$\mu^{(1)} = \frac{1}{3} \left[\frac{H\left(y^{(r)}\right)}{F\left(y^{(r)}\right)} \frac{1}{\sigma_e^2} \right]^{\frac{n-1}{2}} \equiv \hat{\mu}^{(1)}\left(y^{(r)}\right) > 0 \tag{32}$$

and (30) becomes

$$\tilde{U}(\sigma_e) = \frac{\sigma_e^{n+1}}{n+1} \sqrt{\sup_{\substack{y^{(r)} \geq 0 \\ y^{(1)} = 1}} \frac{[F(y^{(r)})]^{n+1}}{[H(y^{(r)})]^{n-1}}} = \frac{\sigma_e^{n+1}}{n+1} \left[\sup_{\substack{y^{(r)} \geq 0 \\ y^{(1)} = 1}} \frac{F\left(y^{(r)}\right)}{H\left(y^{(r)}\right)^{\frac{n-1}{n+1}}} \right]^{\frac{n+1}{2}}. \tag{33}$$

It is interesting to note that the expression for the effective stress potential given in (33) is of the power-law type defined in (3), i.e., when all phases have the same creep exponent n, the effective behavior of the composite is also of the power-law type with creep exponent n implying that $\tilde{U}$ is a homogeneous function of degree $n+1$ in $\boldsymbol{\sigma}$. Also, the optimal values of $y^{(r)}$ in (33) are now *independent* of the macroscopic von Mises equivalent stress σ_e.

Step 3: Perfectly plastic phases $(n \to \infty)$

Using (33) and taking into account that

$$\lim_{n\to\infty} \frac{[a(n)]^{n+1}}{n+1} = \begin{cases} 0 & \text{when } \; a(\infty) \leq 1\,, \\ \infty & \text{when } \; a(\infty) > 1\,, \end{cases} \tag{34}$$

we find

$$\lim_{n\to\infty} \tilde{U}(\sigma_e) = \begin{cases} 0 \quad \text{when} \quad \sigma_e \sqrt{\sup\limits_{\substack{y^{(r)}\geq 0 \\ y^{(1)}=1}} \frac{F\left(y^{(r)}\right)}{H_\infty\left(y^{(r)}\right)}} \leq 1\,, \\ \\ \infty \quad \text{when} \quad \sigma_e \sqrt{\sup\limits_{\substack{y^{(r)}\geq 0 \\ y^{(1)}=1}} \frac{F\left(y^{(r)}\right)}{H_\infty\left(y^{(r)}\right)}} > 1\,, \end{cases} \tag{35}$$

where $F\left(y^{(r)}\right)$ is defined in (26) and

$$H_\infty\left(y^{(r)}\right) = \lim_{n\to\infty} H\left(y^{(r)}\right) = \sum_{r=1}^{N} c^{(r)} {\sigma_0^{(r)}}^2 y^{(r)}. \tag{36}$$

Equation (35) can be written also as

$$\lim_{n\to\infty} \tilde{U}(\sigma_e) = \begin{cases} 0 \quad \text{when} \quad \sigma_e \leq \tilde{\sigma}_0\,, \\ \infty \quad \text{when} \quad \sigma_e > \tilde{\sigma}_0\,, \end{cases} \tag{37}$$

with

$$\boxed{\tilde{\sigma}_0 = \sqrt{\inf_{\substack{y^{(r)}\geq 0 \\ y^{(1)}=1}} \frac{H_\infty\left(y^{(r)}\right)}{F\left(y^{(r)}\right)}}}, \; r = 2, ..., N \tag{38}$$

where $H_\infty\left(y^{(r)}\right)$ and $F\left(y^{(r)}\right)$ are defined in (36) and (26) respectively, i.e.,

$$\boxed{\tilde{\sigma}_0(c^{(r)}, \sigma_0^{(r)}) = \sqrt{\inf_{\substack{y^{(i)}\geq 0 \\ y^{(1)}=1 \\ i=2,...,N}} \left(\sum_{r=1}^{N} c^{(r)} {\sigma_0^{(r)}}^2 y^{(r)}\right) \left(\sum_{p=1}^{N} \frac{c^{(p)}}{3\,y^{(p)} + 2\,y_0}\right) \left(\sum_{s=1}^{N} \frac{c^{(s)}\,y^{(s)}}{3\,y^{(s)} + 2\,y_0}\right)^{-1}}}. \tag{39}$$

Comparing the above equation (37) with (6), we conclude that, when all phases are perfectly plastic ($n = \infty$), the form of the estimated effective stress potential $\tilde{U}(\sigma_e)$ corresponds to a perfectly plastic material that obeys the von Mises yield condition with a flow stress $\tilde{\sigma}_0$ defined in (39). This effective flow stress, in turn, is a function of the phase volume fractions $c^{(r)}$ as well as of the phase flow stresses $\sigma_0^{(r)}$.

Calculation of the estimated effective yield stress $\tilde{\sigma}_0$ requires the solution of the constrained optimization problem in (39) for the values of $y^{(r)}$, which define in turn the appropriate values of the viscosities $\mu^{(r)}$ (see (28)). In the special case of a two-phase composite the solution of the optimization problem in (39) can be found analytically as described in section 3.2.1. The solution of more general cases presented in the following are obtained by using the methodology of Kaufman *et al.* [18] and the CONMAX software (`http://www.netlib.org/opt/conmax.f`) for the solution of the optimization problem in (39).

The optimal values $y^{(r)}$ in (39) depend on the values of the volume fractions $c^{(r)}$ and the flow stresses $\sigma_0^{(r)}$ of the phases but are *independent* of the macroscopic stress state. Also, depending on the parameters of the problem, the optimal values $\hat{y}^{(r)} = \hat{\mu}^{(1)}/\hat{\mu}^{(r)}$ may be one of the extreme values 0 or ∞. The value $\hat{y}^{(r)} = 0$ corresponds to a rigid comparison material for phase r, whereas $\hat{y}^{(r)} = \infty$ corresponds to an incompressible comparison material with

zero stiffness (i.e., to an "incompressible void" comparison material). It should be noted that it is possible to have $\hat{y}^{(r)} = \hat{\mu}^{(1)}/\hat{\mu}^{(r)} = 0$ (rigid comparison material) even for finite $\sigma_0^{(r)}$ (e.g., see deBottton and Ponte Castañeda [8] and section 3.2.1 below).
The strain concentration values $\alpha^{(r)}$ defined in (20) can be written in the form

$$\boxed{\alpha^{(r)} = \frac{\hat{y}^{(r)}}{3\,\hat{y}^{(r)} + 2\,y_0}\left(\sum_{s=1}^{N} \frac{c^{(s)}\,\hat{y}^{(s)}}{3\,\hat{y}^{(s)} + 2\,y_0}\right)^{-1}}, \tag{40}$$

where $\hat{y}^{(r)}$ are the optimal values of $y^{(r)}$ resulting from the optimization in (39).

3.2.1 The two-phase perfectly plastic composite — An analytic estimate for the effective flow stress and the strain concentration factors

We consider an isotropic two-phase composite ($N = 2, c_1 + c_2 = 1$). Each phase is perfectly plastic with flow stress $\sigma_0^{(1)}$ and $\sigma_0^{(2)}$. We treat phase 1 as the "matrix" and phase 2 with $\sigma_0^{(2)} > \sigma_0^{(1)}$ as the reinforcing particles. In that case it is possible to obtain analytical expressions for the effective flow stress $\tilde{\sigma}_0$.
The estimate for $\tilde{\sigma}_0$ depends on the chosen value of the reference viscosity μ_0 in (13). Results for various choices of μ_0 are reported in Papadioti [27] and will be discussed briefly later in this section. Here we present in some detail the formulation based on a Hashin-Strikman lower bound with $\mu_0 = \mu^{(1)}$ ($y_0 = 1$); as it will be discussed in the following section 4, this particular choice of μ_0 shows the best agreement with detailed unit cell finite element calculations. For $\mu_0 = \mu^{(1)}$, the ratio H_∞/F in (38) takes the value

$$\frac{H_\infty\left(y^{(2)}\right)}{F\left(y^{(2)}\right)} = {\sigma_0^{(1)}}^2\left(c^{(1)} + c^{(2)}\,r^2\,y^{(2)}\right)\frac{2 + 3\,c^{(2)} + 3\,c^{(1)}\,y^{(2)}}{2\,c^{(1)} + (3 + 2\,c^{(2)})\,y^{(2)}}, \qquad r = \frac{\sigma_0^{(2)}}{\sigma_0^{(1)}} > 1. \tag{41}$$

The optimum value of $y^{(2)}$ to be used in (38) is calculated by using the condition

$$\frac{\partial}{\partial y^{(2)}}\left(\frac{H_\infty}{F}\right) = 0 \tag{42}$$

together with the constraint $y^{(2)} \geq 0$. After some lengthy, but straightforward, calculations we find the resulting optimal value $\hat{y}^{(2)}$ to be

$$\hat{y}^{(2)} = \begin{cases} \frac{1}{3+2\,c^{(2)}}\left[-2\,c^{(1)} + \frac{5}{\sqrt{3}}\sqrt{(3 + 2\,c^{(2)})\,\frac{1}{r^2} - 2\,c^{(2)}}\right] & \text{if } \; 1 \leq r \leq r_{\rm cr} \quad \left(c^{(2)} \leq c^{(2)}_{\rm cr}\right), \\ 0 & \text{if } \; r \geq r_{\rm cr} \qquad \left(c^{(2)} \geq c^{(2)}_{\rm cr}\right), \end{cases} \tag{43}$$

where

$$r_{\rm cr} = \frac{5}{\sqrt{4 + 6\,c^{(2)}}} \qquad \text{and} \qquad c^{(2)}_{\rm cr} = \frac{1}{6}\left[\left(\frac{5}{r}\right)^2 - 4\right]. \tag{44}$$

According to (43), for a given particle concentration $c^{(2)}$, when the contrast ratio $r = \sigma_0^{(2)}/\sigma_0^{(1)}$ is larger than a value $r_{\rm cr}$, the comparison material for phase 2 (particles) is rigid ($\hat{y}^{(2)} = 0$).

The corresponding estimate for the effective flow stress resulting from (38) is

$$\boxed{\frac{\tilde{\sigma}_0}{\sigma_0^{(1)}} = \begin{cases} \frac{1}{3+2\,c^{(2)}}\left(5\,c^{(2)}\,r + c^{(1)}\sqrt{9+6\,c^{(2)}(1-r^2)}\right) & \text{if} \quad 1 \le r \le r_{\rm cr} \quad \left(c^{(2)} \le c^{(2)}_{\rm cr}\right), \\ \frac{1}{2}\sqrt{4+6\,c^{(2)}} & \text{if} \quad r_{\rm cr} \le r \quad \left(c^{(2)}_{\rm cr} \le c^{(2)}\right). \end{cases}} \tag{45}$$

The result stated in (45) was first presented by deBottton and Ponte Castañeda [8], who used a "dissipation function" formulation (as opposed to the "stress potential" approach used here). For all volume fractions $c^{(2)}$, there is a value $r_{\rm cr}$ of the contrast ratio $r = \sigma_0^{(2)}/\sigma_0^{(1)}$ beyond which the predicted effective flow stress $\tilde{\sigma}_0$ does not vary with r. For values of r larger than $r_{\rm cr}$, the optimal value of $y^{(2)} = \mu^{(1)}/\mu^{(2)}$ vanishes or $\mu^{(2)} = \infty$, i.e., for $r \ge r_{\rm cr}$ the comparison material 2 (particles) does not deform; therefore, further increase of $\sigma_0^{(2)}$ does not change the effective flow stress $\tilde{\sigma}_0$.

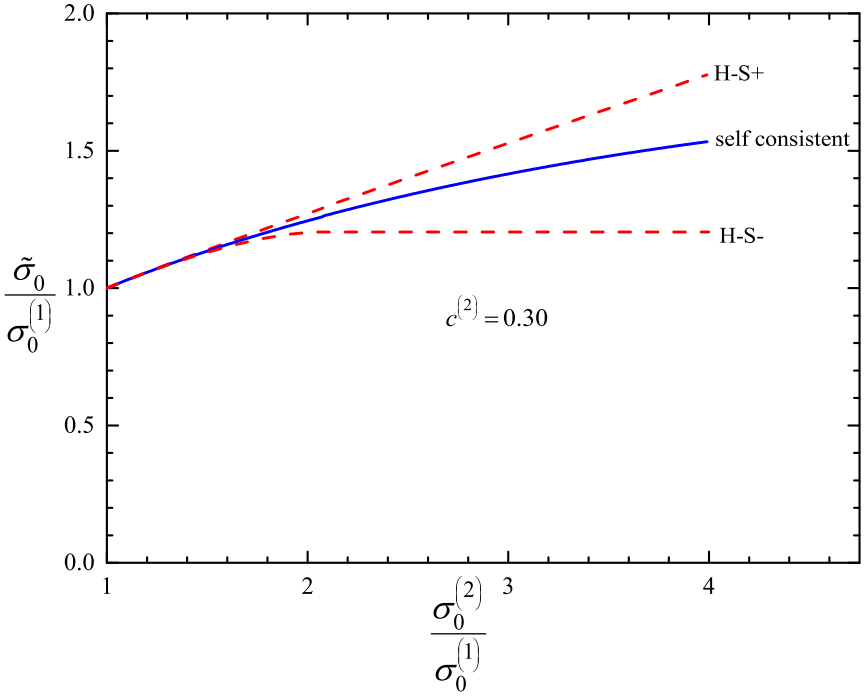

Figure 1: Variation of effective normalized flow stress $\tilde{\sigma}_0/\sigma_0^{(1)}$ with contrast ratio $r = \sigma_0^{(2)}/\sigma_0^{(1)}$ as predicted by various models for a volume fraction $c^{(2)} = 0.30$.

The estimate for the effective flow stress $\tilde{\sigma}_0$ depends on the choice of the reference viscosity μ_0. Figure 1 shows the predicted $\tilde{\sigma}_0$ for various choices of μ_0 for a volume fraction $c^{(2)} = 0.30$. The curves marked H-S$^-$ and H-S$^+$ correspond to $\mu_0 = \mu^{(1)}$ and $\mu_0 = \mu^{(2)}$ respectively, and "self consistent" corresponds to $\mu_0 = \tilde{\mu}$. We emphasize that the Hashin-Shtrikman lower bound H-S$^-$ ($\mu_0 = \mu^{(1)}$) shows the best agreement with detailed unit cell finite element calculations presented in the following section.

The strain concentration values $\alpha^{(r)}$ given in (29) can be written in the form

$$\boxed{\alpha^{(1)} = \frac{d\bar{\varepsilon}^{(1)}}{d\bar{\varepsilon}} = \frac{1}{(2\,y_0+3)\,\mathcal{D}}}, \qquad \boxed{\alpha^{(2)} = \frac{d\bar{\varepsilon}^{(2)}}{d\bar{\varepsilon}} = \frac{\hat{y}^{(2)}}{(2\,y_0+3\,\hat{y}^{(2)})\,\mathcal{D}}}, \tag{46}$$

where

$$\boxed{\mathcal{D} = \frac{c^{(1)}}{2\,y_0 + 3} + \frac{c^{(2)}\,\hat{y}^{(2)}}{2\,y_0 + 3\,\hat{y}^{(2)}}} \tag{47}$$

and $\hat{y}^{(2)}$ is defined in (43).

4 Unit cell finite element calculations and assessment of the models

In this section we present the results of unit cell finite element calculations for a composite material made up of a statistically isotropic random distribution of isotropic, linearly-elastic perfectly-plastic spherical inclusions embedded in a continuous, isotropic, linearly-elastic perfectly-plastic matrix. The elastic Young modulus used in the finite element calculations for all phases is three orders of magnitude higher than the highest yield stress involved; this minimizes the effects of elasticity and the results are very close to those of rigid-perfectly-plastic materials.

We study numerically two- and three-phase composites. The matrix is labelled as phase 1 and the reinforcing particles are spherical and have higher flow stresses ($\sigma_0^{(i)} > \sigma_0^{(1)}, i > 1$). The periodic unit cell is a cube with edge size L and is constructed using the method presented by Segurado and Llorca [39] (see also [10]) and extended to polydisperse inclusion distributions by Lopez-Pamies et al. [21]. The virtual microstructure contains a dispersion of a sufficiently large number of non-overlapping spheres of uniform (monodisperse) or different (polydisperse) size. The inclusions are randomly located within the cell and are generated using the Random Sequential Adsorption Algorithm (RSA) [38]. In addition, the unit cell is periodic, i.e., it can be repeated in all three directions to represent a 3-D periodic structure. For the two-phase composite and for $c^{(2)} \leq 0.20$ monodisperse spheres are used; for higher volume fractions polydisperse (variable size) distributions are used. In the present study, the two-phase polydisperse approach of Lopez-Pamies et al. [21] is readily extended to obtain virtual microstructures with three-phases or more. For instance, denoting the matrix phase with 1 and the two inclusion phases with 2 and 3, the extension is straightforward and requires the continuous alternation of spheres of phase 2 and spheres of phase 3 during the RSA process. Of course this simple extension can be repeated as often as necessary to obtain an $N-$phase virtual microstructure provided that the concentration of each of the phases is known. Moreover, as discussed briefly in the following, a convergence study with respect to the number of spheres is done for all virtual microstructures used in this study to ensure isotropy and ergodicity of the virtual unit cell.

Finite element discretizations of the cubic unit cell were created from the particle center distributions using the mesh generator code NETGEN [40], which has the capability to create periodic meshes as required. All calculations were carried out using the ABAQUS general purpose finite element code (Hibbitt [13]). Three dimensional 10-node quadratic tetrahedral elements with a constant pressure interpolation were used (C3D10H in ABAQUS); all analyses were carried out incrementally and accounted for geometry changes due to deformation (finite strain solutions).

Figure 2 shows the finite element meshes used for a two-phase composite with volume fractions $c^{(2)}$ =0.10, 0.20, 0.30, and 0.40. The distributions are monodisperse for $c^{(2)}$ =0.10 and 0.20, and polydisperse for $c^{(2)}$ =0.30 and 0.40. Figure 3 shows a typical finite element mesh

of a unit cell for a three-phase polydisperse composite for a matrix with volume fraction $c^{(1)} = 0.60$ and two different inclusion types with $c^{(2)} = 0.25$ and $c^{(3)} = 0.15$.

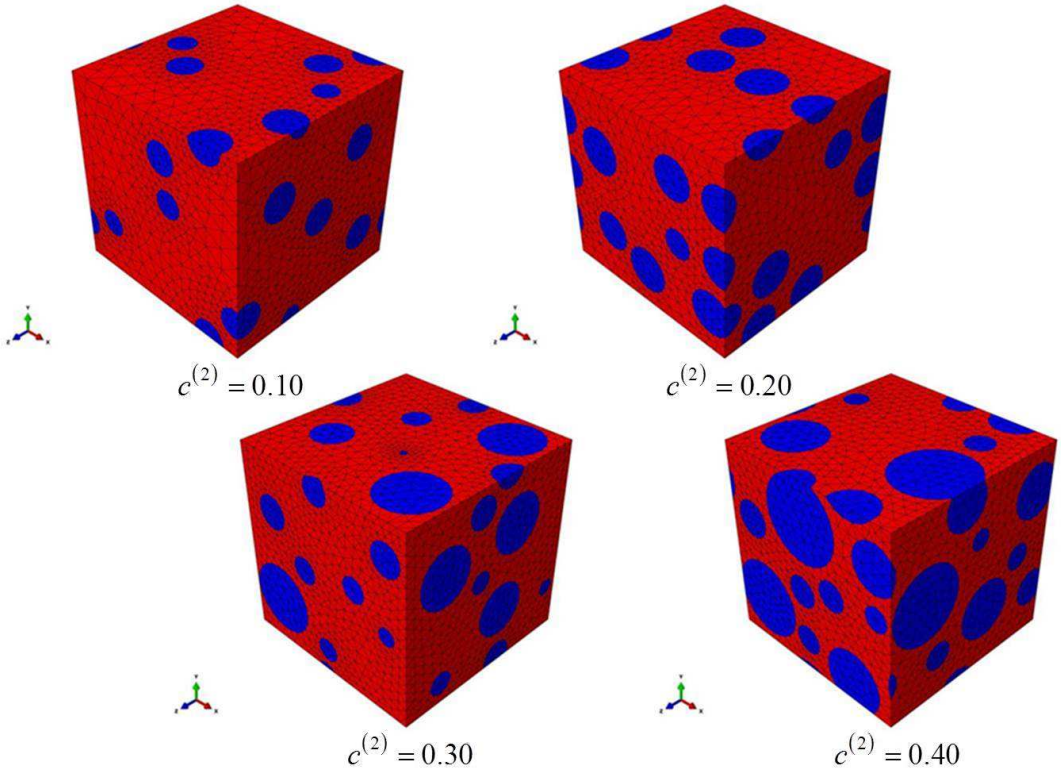

Figure 2: Finite element discretization of cubic unit cells for two-phase composites containing a random distribution of 30 spherical particles for volume fractions of 10, 20, 30 and 40%. The finite element meshes have (200,869; 112,281; 165,371; 159,303) nodes and (83,270; 45,679; 67,790; 65,543) elements respectively. The corresponding total numbers of degrees of freedom, including pressures, are (436,067; 245,485; 360,533; 346,823).

4.1 The effective yield stress

We determine numerically the effective yield stress by solving the problem of a unit cell loaded in uniaxial tension. Periodicity conditions are imposed on the boundary of the unit cell. A detailed discussion of the periodic boundary consitions on a unit cell can be found in Suquet [41] or Michel *et al.* [26]. Here, the periodic boundary conditions on the unit cell are imposed as follows (see Mbiakop *et al.* [23] and Papadioti [27] for more details). Referring to Fig. 4, if we fix vertex 1 in order to eliminate rigid body translations, then, in view of the periodicity of the displacement field, we can write the displacements $\mathbf{u}$ at vertices 2, 4, and 5 of the unit cell in the form

$$u_i^{(2)} = (F_{i1} - \delta_{i1})\, L, \qquad u_i^{(4)} = (F_{i2} - \delta_{i2})\, L, \qquad u_i^{(5)} = (F_{i3} - \delta_{i3})\, L, \tag{48}$$

where F_{ij} are the components of the macroscopic deformation gradient $\mathbf{F}$. The periodicity of the problem requires also that the displacements of material points at the same position on opposite faces of the cell should satisfy the conditions

$$\mathbf{u}^{\text{RIGHT}} - \mathbf{u}^{\text{LEFT}} = \mathbf{u}^{(2)}, \qquad \mathbf{u}^{\text{TOP}} - \mathbf{u}^{\text{BOTTOM}} = \mathbf{u}^{(4)}, \qquad \mathbf{u}^{\text{FRONT}} - \mathbf{u}^{\text{BACK}} = \mathbf{u}^{(5)}, \tag{49}$$

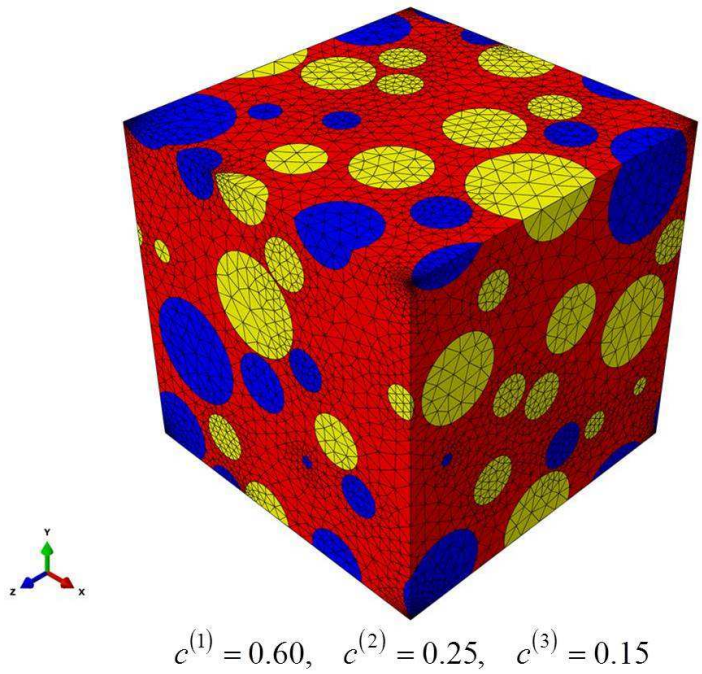

Figure 3: Finite element discretization of a cubic unit cell for a three-phase composite containing a random distribution of 30 polydisperse spherical particles with volume fractions $c^{(2)} = 0.25$ (yellow) and $c^{(3)} = 0.15$ (blue). The finite element mesh has 303,953 nodes, 124,225 elements, and the total number of degrees of freedom, including pressures, is 663,409.

where the superscripts (LEFT, RIGHT), (BOTTOM, TOP), and (BACK, FRONT) denote collectively all material points located respectively on the faces of the cell at $(X_1 = 0, X_1 = L)$, $(X_2 = 0, X_2 = L)$, and $(X_3 = 0, X_3 = L)$. Equations (49) show that the periodic constraints between all corresponding opposite boundary points can be written in terms of the displacements of the three vertex points $(\mathbf{u}^{(2)}, \mathbf{u}^{(4)}, \mathbf{u}^{(5)})$, which are defined, in turn, in (48) by the macroscopic deformation gradient $\mathbf{F}$. In ABAQUS, for given $\mathbf{F}$, we impose boundary conditions on $(\mathbf{u}^{(2)}, \mathbf{u}^{(4)}, \mathbf{u}^{(5)})$ according to (48), and the periodicity constraints (49) are enforced through a "user MPC" subroutine (or the "EQUATION" option).

For the problem of uniaxial tension in direction 1, the deformation gradient is of the form

$$\mathbf{F} = \lambda\, \mathbf{e}_1\, \mathbf{e}_1 + \lambda_t(\mathbf{e}_2\, \mathbf{e}_2 + \mathbf{e}_3\, \mathbf{e}_3), \tag{50}$$

where (λ, λ_t) are the axial and transverse stretch ratios and $\mathbf{e}_i$ the base vectors along the coordinate axes shown in Fig. 4; the boundary conditions (48) become

$$u_1^{(2)} = (\lambda - 1)\, L, \qquad u_2^{(4)} = u_3^{(5)} = (\lambda_t - 1)\, L, \tag{51}$$

$$u_2^{(2)} = u_3^{(2)} = \quad u_1^{(4)} = u_3^{(4)} = \quad u_1^{(5)} = u_2^{(5)} = 0. \tag{52}$$

In ABAQUS, we prescribe $u_1^{(2)}$ (i.e., λ) and set $R_2^{(4)} = R_3^{(5)} = 0$, where $R_i^{(N)}$ denotes the i-th component of the force at node N. The quantities $R_1^{(2)}$ and $(u_2^{(4)}, u_3^{(5)})$, i.e., λ_t, are determined by the finite element solution. The corresponding macroscopic stresses σ_{ij} are determined

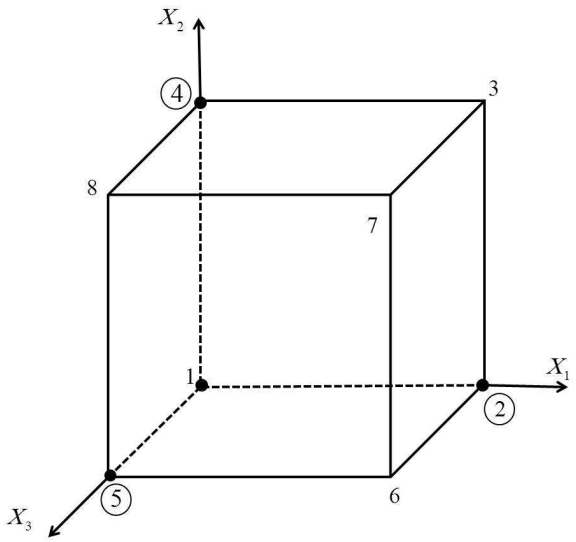

Figure 4: Periodic unit cell.

from the numerical calculation of the average stresses $< \sigma_{ij} >$ in the finite element solution:[3]

$$< \sigma_{ij} >= \frac{1}{V_{\text{cell}}} \int\limits_{V_{\text{cell}}} \sigma_{ij}(\mathbf{x})\, dV, \tag{53}$$

where V_{cell} is the total volume of the deformed finite element mesh.
The conditions $u_2^{(4)} = u_3^{(5)}$ and $< \sigma_{22} >=< \sigma_{33} >=< \sigma_{12} >=< \sigma_{13} >=< \sigma_{23} >= 0$ are used to verify the correctness of the finite element solution.
The nodal displacement $u_1^{(2)}$ was increased gradually, the solution was developed incrementally, and the average stress $< \sigma_{11} >$ was determined by (53) at the end of every increment. As $u_1^{(2)}$ increases, the calculated average stress $< \sigma_{11} >$ reaches a constant value, which defines the effective flow stress of the composite $\tilde{\sigma}_0$.
Figure 5 shows the variation of the calculated effective flow stress from the unit cell finite element calculations with the contrast ratio $r = \sigma_0^{(2)}/\sigma_0^{(1)}$ for various volume fractions, together with the predictions (39) of the homogenization model, based on he Hashin-Shtrikman lower bound H-S$^-$ ($\mu_0 = \mu^{(1)}$).[4] For that data shown in Fig. 5, the maximum difference between the predictions (39) and the results of the unit cell finite element calculations is 3% (note that the vertical axis in Fig. 1 starts at the value of 1). It is also interesting to mention that an increase of the flow stress $\sigma_0^{(2)}$ in the inclusions beyond (approximately) two times the flow stress of the matrix ($2\,\sigma_0^{(1)}$) does not change the effective flow stress of the composite for all volume fractions considered here. The finite element calculations confirm the fact that, for $\sigma_0^{(2)} \gtrsim 2\,\sigma_0^{(1)}$, the inclusions do not deform plastically in the deforming unit cell and are in agreement with earlier numerical results of Suquet [44] for $c^{(2)} = 30\%$ and by Ponte Castañeda and Suquet [36] and Idiart *et al.* [15] for $c^{(2)} = 15\%$. As we will see in

[3] The alternative calculation $< \sigma_{11} >= R_1^{(2)}/A_{\text{cell}}$ appears to be less convenient as it requires evaluation of the current cross sectional area of the deformed cell A_{cell} which in general does not remain flat due to the complex microstructure of the unit cell.

[4] Of all possible choices for μ_0 shown in Fig. 1, the Hashin-Shtrikman lower bound H-S$^-$ ($\mu_0 = \mu^{(1)}$) gives the best estimate by comparison to the predictions of the unit cell results.

the following, this result is due to the fact that the particles behave as being rigid beyond further increase of $\sigma_0^{(2)}$.

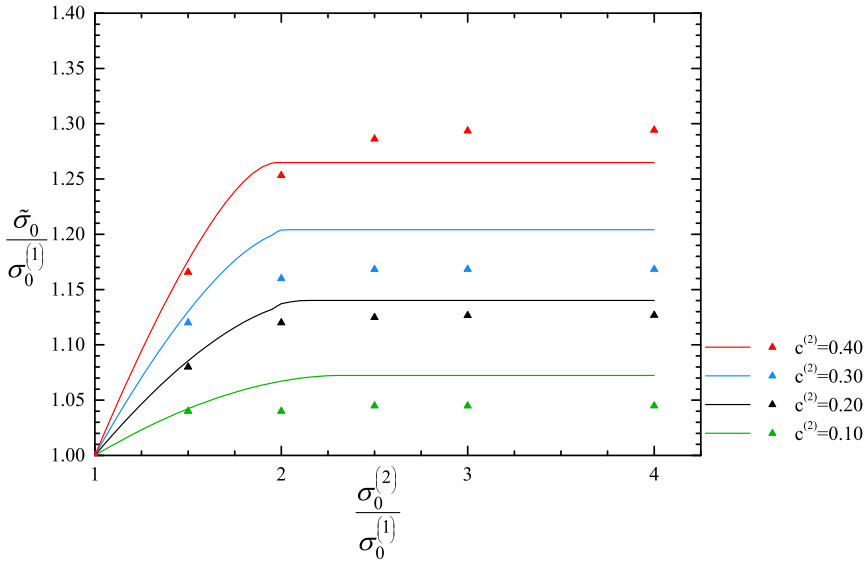

Figure 5: Variation of normalized effective flow stress $\tilde{\sigma}_0/\sigma_0^{(1)}$ with contrast ratio $r = \sigma_0^{(2)}/\sigma_0^{(1)}$ for different values of the volume fraction $c^{(2)}$. The full triangles are the results of the unit cell finite element calculations and the solid lines are the predictions (39) of the model based on the H-S$^-$ estimate ($\mu_0 = \mu^{(1)}$). The maximum difference between the numerical results and the analytical estimates is 3%.

Figure 6 shows the variation of $\tilde{\sigma}_0/\sigma_0^{(1)}$ of a three-phase composite for different values of the volume fraction $c^{(3)}$ as determined from the unit cell finite element calculations and the predictions (39) of the homogenization model. The material data are typical for a TRIP [5] steel with a ferritic matrix (phase 1) containing retained austenite (phase 2), which transforms gradually to martensite (phase 3) as the TRIP steel deforms plastically (e.g., see Papatriantafillou *et al.* [28]).
In order to check the isotropy of the unit cell, we carried out calculations for uniaxial tension in directions 2 and 3. In all cases, the results were identical to those shown in Figs. 5 and 6.

4.2 The strain concentration tensors

The unit cell finite element calculations discussed above were used also to determine the strain concentration factors defined in (20) as follows. At the end of every increment in the finite element solution the average value of the Eulerian logarithmic strain tensor $\boldsymbol{\varepsilon}^{(r)}$ was determined in every phase of the composite, where the superscript (r) denotes "phase r". The macroscopic axial logarithmic strain was also determined as $\bar{\varepsilon} = \ln \lambda$, where λ is the axial stretch ratio used in (51) to drive the finite element calculations. Interestingly, the components of $< \boldsymbol{\varepsilon}^{(r)} >$ are found to be proportional to $\bar{\varepsilon}$ in the context of the present study; in particular, it is found that

$$< \varepsilon_{ij}^{(r)} >= C_{ij}\, \bar{\varepsilon}, \tag{54}$$

[5] TRIP is the acronym for **TR**ansformation **I**nduced **P**lasticity.

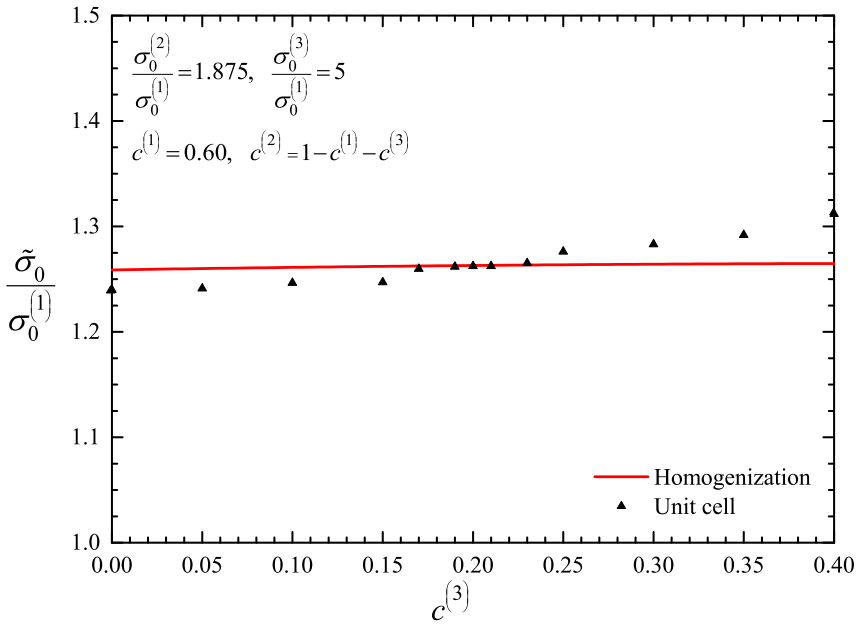

Figure 6: Variation of effective normalized flow stress $\tilde{\sigma}_0/\sigma_0^{(1)}$ of a three-phase composite with a matrix volume fraction $c^{(1)} = 0.60$ for different values of the volume fraction $c^{(3)}$. The homogenization estimates are based on H-S$^-$ and the contrast ratios are $\sigma_0^{(2)}/\sigma_0^{(1)} = 1.875$ and $\sigma_0^{(3)}/\sigma_0^{(1)} = 5$.

which leads to the following estimate for the strain concentration $\alpha^{(r)}$:

$$\alpha^{(r)} = \frac{d\bar{\varepsilon}^{(r)}}{d\bar{\varepsilon}} = \sqrt{\frac{2}{3}\, C_{ij}\, C_{ij}}. \tag{55}$$

Figure 7 shows the variation of the strain concentration factors $\alpha^{(r)}$ in a two-phase composite with the contrast ratio $r = \sigma_0^{(2)}/\sigma_0^{(1)}$ for various volume fractions as determined from the unit cell finite element calculations (equation (54)) and the homogenization theory (equations (46)—(47)).

An important observation in the context of this figure is that at a contrast ratio of $r \simeq 2$, a sharp transition is observed where the particles start behaving as being rigid, i.e., the average strain in the particle is almost zero. This is validated by both the model and the numerical results. In terms of the homogenization procedure, this implies that the case of infinite contrast, i.e., rigid particles, and finite contrast is very similar beyond a value of $r \simeq 2$. A weak dependence of this sharp transition upon the volume fraction c is observed in these figures.

Similar plots for a three-phase composite are shown in Fig. 8. The predictions of homogenization theory agree well with the results of the unit cell finite element calculations.

Figure 8 shows, in turn, the strain concentration factors in a three-phase material. The comparison between the model and the finite element simulations is qualitatively good, whereas the model tends to underestimate the straining of the middle phase, i.e., the one with yield stress $\sigma_0^{(2)}/\sigma_0^{(1)} = 1.875$. Again, in the case of the third phase, when $\sigma_0^{(3)}/\sigma_0^{(1)} = 5$, the particle behaves as rigid which is consistent with the observations of the previous figure.

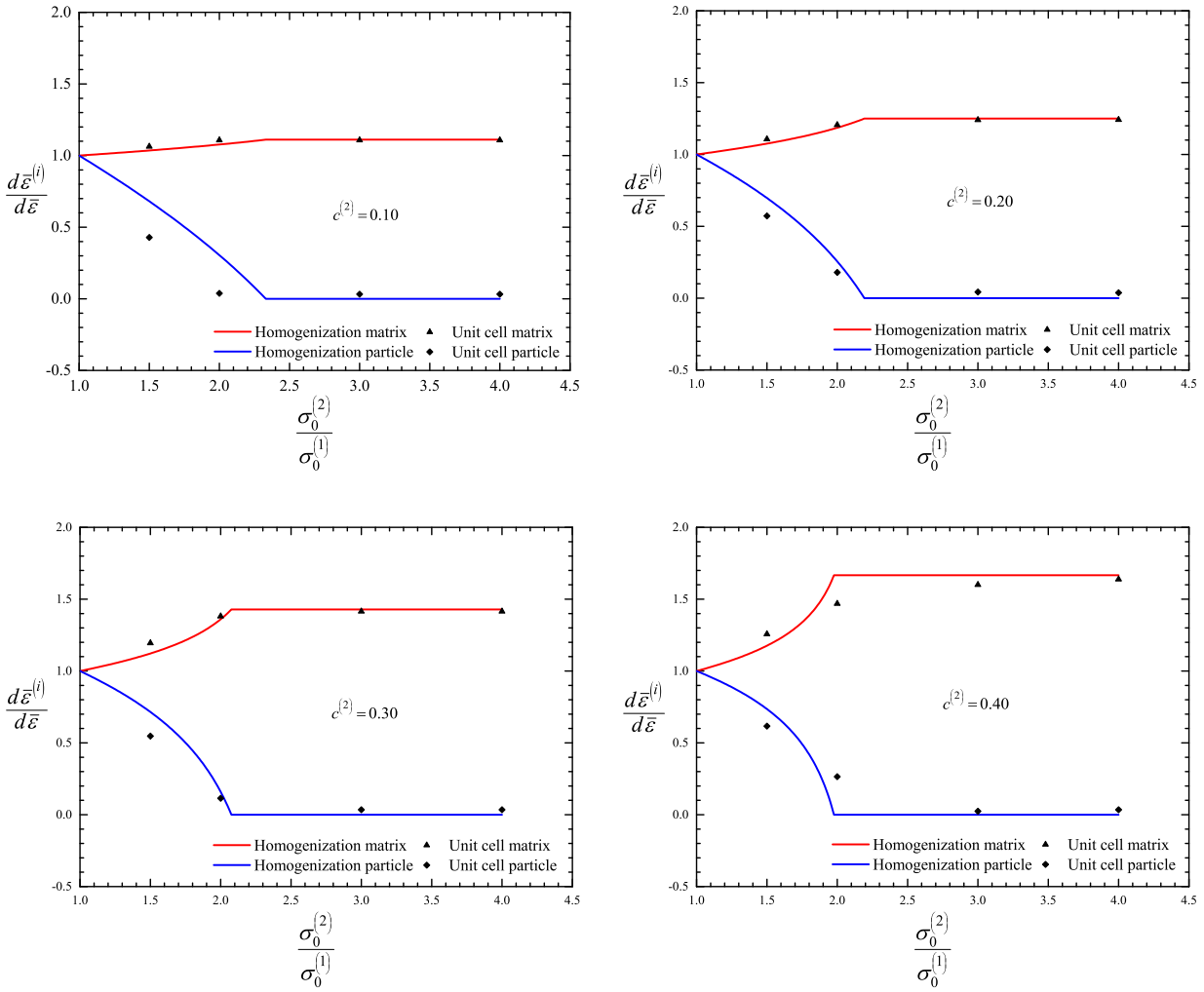

Figure 7: Strain concentration factors $\alpha^{(i)} = d\bar{\varepsilon}^{(i)}/d\bar{\varepsilon}$ as determined from unit cell finite element calculations and homogenization theory (equations (46) and (47)) for a two-phase composite.

4.3 On the possible dependence of the effective flow stress on J_3

Suquet and Ponte Castañeda [42, 35] studied the effective mechanical behavior of weakly inhomogeneous composites and showed that, for the case of incompressible "power-law" phases, the effective potential of the composite may depend, to second order, on the third invariant of the applied strain.

We carry out detailed unit cell finite element calculations in order to check for a possible dependence of the effective yield stress $\tilde{\sigma}_0$ on the third invariant J_3 of the stress deviator $\mathbf{s}$ ($J_3 = \det\mathbf{s}$, where 'det' denotes the determinant). We identify the coordinate axes shown in Fig. 4 with the principal directions of the stress tensor and write the principal stresses in the form

$$\left\{ \begin{array}{c} \sigma_1 \\ \sigma_2 \\ \sigma_3 \end{array} \right\} = \sigma_e \left(X_\Sigma \left\{ \begin{array}{c} 1 \\ 1 \\ 1 \end{array} \right\} + \frac{2}{3} \left\{ \begin{array}{c} \cos\left(\theta + \frac{\pi}{6}\right) \\ \sin\theta \\ -\cos\left(\theta - \frac{\pi}{6}\right) \end{array} \right\} \right), \tag{56}$$

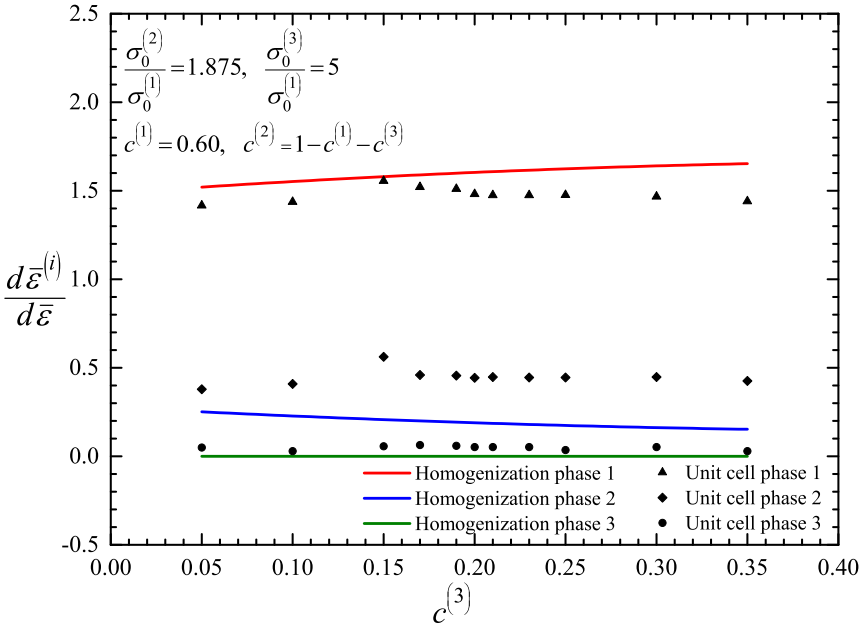

Figure 8: Strain concentration factors $\alpha^{(i)} = d\bar{\varepsilon}^{(i)}/d\bar{\varepsilon}$ as determined from unit cell finite element calculations and homogenization theory (equation (40)) for a three-phase composite.

where $X_\Sigma = p/\sigma_e$ is the stress triaxiality and θ is the "Lode angle", so that

$$J_3 = \det \mathbf{s} = -\frac{2}{27}\,\sigma_e^3\,\sin 3\theta. \tag{57}$$

Angle θ takes values in the range $-30^\circ \le \theta \le 30^\circ$, where, to within a given hydrostatic stress, $\theta = -30^\circ$ corresponds to uniaxial tension, $\theta = 0$ to pure shear, and $\theta = 30^\circ$ to uniaxial compression.

It is stressed at this point that the composite materials considered in this work are plastically incompressible and thus the applied stress triaxiality affects only the elastic part which is of no interest here. Thus the only relevant invariant studied in this section, apart from the J_2 invariant, is the third deviatoric invariant J_3 defined above. The study of the effect of J_3, in turn, allows for a complete analysis of general triaxial loading states.

As a consequence of the applied periodic boundary conditions and the symmetry of the problem, the macroscopic (average) deformation of the unit cell is entirely described by the displacements of the "reference vertices" (2,4,5), as shown in Fig. 4, which can be written in the form

$$\mathbf{u}^{(2)} = U_1\,\mathbf{e}_1, \qquad \mathbf{u}^{(4)} = U_2\,\mathbf{e}_2, \qquad \mathbf{u}^{(5)} = U_3\,\mathbf{e}_3. \tag{58}$$

In ABAQUS, the displacements (U_1, U_2, U_3) are tied, through "user multipoint constraints", to the degrees of freedom of a fictitious node, which is properly displaced so that the desired triaxiality X_Σ and Lode angle θ are achieved. Details of the numerical formulation can be found in Mbiakop *et al.* [23, 24] (see also Barsoum and Faleskog [2] and Papadioti [27]).

We carry out finite element calculations in which the unit cell is loaded with $X_\Sigma = 1/3$ and Lode angles in the range $-30^\circ \le \theta \le 30^\circ$. The finite element analysis is carried out incrementally; at the end of each increment the average stress $<\boldsymbol{\sigma}>$ and the corresponding von Mises equivalent stress $\bar{\sigma}_e = \sqrt{\frac{3}{2} <\mathbf{s}>:<\mathbf{s}>}$ are calculated. As the applied displacement

of the fictitious node increases, $\bar{\sigma}_e$ takes a constant value, which defines the effective flow stress $\tilde{\sigma}_0$ of the periodic composite.
In order to verify that the desired values have been indeed achieved, the triaxiality and Lode angle corresponding to the average stress $< \boldsymbol{\sigma} >$ are determined at the end of every increment. Also, since the coordinate axes in the finite element solution are assumed to coincide with the principal stress directions, the conditions $< \sigma_{12} >=< \sigma_{13} >=< \sigma_{23} >= 0$ are checked at the end of every increment to verify the accuracy of the finite element solution. Figure 9 shows the variation of the effective flow stress $\tilde{\sigma}_0$, as determined from unit cell finite element calculations, with Lode angle θ for particle volume fractions $c^{(2)}$ =0.10, 0.20, 0.30, and 0.40. Figure 9 shows that the effective flow stress of the composite is essentially independent of the third stress invariant J_3, which is in agreement with earlier results by Suquet [44], Ponte Castañeda and Suquet [36] and Idiart [16] in the case of rigid particles.

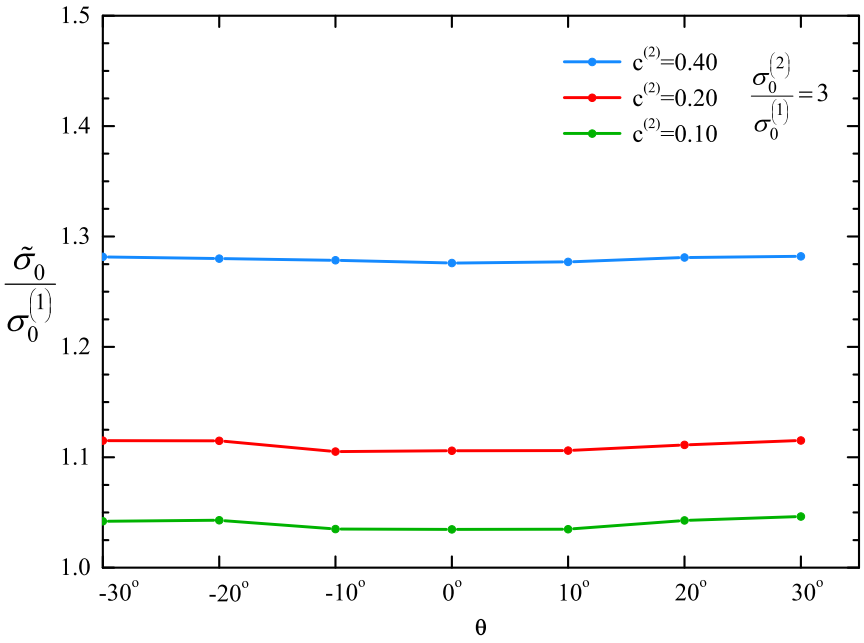

Figure 9: Variation of effective normalized flow stress $\tilde{\sigma}_0/\sigma_0^{(1)}$ with Lode angle θ for particle volume fractions of 10, 20, 30, and 40%. The results show almost no depedence on J_3.

==

5 Hardening phases

In this section we present an approximate method for the prediction of the incremental elastoplastic behavior of macroscopically isotropic composites made of N isotropic, rate-independent, elastic-plastic *hardening* phases. Let the flow stresses $\sigma_y^{(i)}$ of each phase be known functions of the corresponding equivalent plastic strains $\bar{\varepsilon}^{(i)}$ $(i = 1, 2, \ldots, N)$. At every point of the homogenized composite the "internal variables" that characterize the local state of the homogenized continuum are the local values of the equivalent plastic strains in the phases $\mathbf{q} = \left(\bar{\varepsilon}^{(1)}, \bar{\varepsilon}^{(2)}, \cdots, \bar{\varepsilon}^{(N)}\right)$.
For simplicity, we consider infinitesimal displacement gradients (small strains and rotations); the method is easily extended to cover the case of finite geometry changes as discussed in

Appendix. The elastic and plastic response of the homogenized composite are treated independently, and combined later to obtain the full elastic-plastic response. The infinitesimal strain tensor $\boldsymbol{\varepsilon}$ at every point in the homogenized material is written as

$$\boldsymbol{\varepsilon} = \boldsymbol{\varepsilon}^e + \boldsymbol{\varepsilon}^p, \tag{59}$$

where $\boldsymbol{\varepsilon}^e$ and $\boldsymbol{\varepsilon}^p$ are the elastic and plastic parts. Linear isotropic elastic behavior is assumed:

$$\boldsymbol{\varepsilon}^e = \boldsymbol{\mathcal{M}}^e : \boldsymbol{\sigma} \qquad \text{or} \qquad \boldsymbol{\sigma} = \boldsymbol{\mathcal{L}}^e : \boldsymbol{\varepsilon}^e, \tag{60}$$

where $\boldsymbol{\mathcal{M}}^e$ is the isotropic elastic compliance tensor, which is the inverse of the isotropic elasticity tensor $\boldsymbol{\mathcal{L}}^e$:

$$\boldsymbol{\mathcal{L}}^e = 2\,\mu\,\boldsymbol{\mathcal{K}} + 3\,\kappa\,\boldsymbol{\mathcal{J}}, \qquad \boldsymbol{\mathcal{M}}^e = (\boldsymbol{\mathcal{L}}^e)^{-1} = \frac{1}{2\,\mu}\,\boldsymbol{\mathcal{K}} + \frac{1}{3\,\kappa}\,\boldsymbol{\mathcal{J}}, \tag{61}$$

and μ and κ denote the effective elastic shear and bulk moduli of the composite.
Let t be a loading (time-like) parameter and consider an infinitesimal change from t_n to $t_{n+1} = t_n + \Delta t$, where Δt is "small". We use the notation A_n and A_{n+1} to denote the values of A at the start t_n and the end t_{n+1} of the increment and set $\Delta A = A_{n+1} - A_n$. We assume that the effective flow stress is, to a first approximation, constant over the period (t_n, t_{n+1}) and can be determined by the optimization problem in (39), in which the flow stresses of the phases take values

$$\sigma_0^{(i)} = (1-\beta)\,\sigma_0^{(i)}\Big|_n + \beta\;\sigma_0^{(i)}\Big|_{n+1}, \qquad 0 \le \beta \le 1. \tag{62}$$

where

$$\sigma_0^{(i)}\Big|_n = \sigma_y^{(i)}\left(\bar{\varepsilon}_n^{(i)}\right) \qquad \text{and} \qquad \sigma_0^{(i)}\Big|_{n+1} = \sigma_y^{(i)}\left(\bar{\varepsilon}_{n+1}^{(i)}\right) = \sigma_y^{(i)}\left(\bar{\varepsilon}_n^{(i)} + \Delta\bar{\varepsilon}^{(i)}\right). \tag{63}$$

Put in other words, the composite is assumed to behave as "incrementally perfectly plastic" with a flow stress $\tilde{\sigma}_0(\mathbf{q}_{n+1})$, which is updated at every increment. The value of $\tilde{\sigma}_0(\mathbf{q}_{n+1})$ is calculated by the solution of the corresponding optimization problem (39) using the $\sigma_0^{(i)}$ values defined in (62). The solution of the optimization problem (39) defines also the optimal values $\hat{y}^{(r)}(\mathbf{q}_{n+1})$, which determine the corresponding strain concentration factors $\alpha^{(i)}$ in (40) for the increment. The actual calculation is implicit in general, except when $\beta = 0$ is used in (62).
Over any time increment (t_n, t_{n+1}) the effective yield condition of the composite is written in the form

$$\Phi\left(\boldsymbol{\sigma}, \mathbf{q}_{n+1}\right) = \sigma_e - \tilde{\sigma}_0\left(\mathbf{q}_{n+1}\right) = 0, \tag{64}$$

where $\tilde{\sigma}_0\left(\mathbf{q}_{n+1}\right)$ is determined from the solution of the optimization problem (39) with $\sigma_0^{(i)}$ defined in (62), and the associated flow rule is

$$\dot{\boldsymbol{\varepsilon}}^p = \dot{\bar{\varepsilon}}\,\mathbf{N}, \qquad \mathbf{N} = \frac{3}{2\,\sigma_e}\,\mathbf{s}, \tag{65}$$

where $\dot{\bar{\varepsilon}} = \sqrt{\frac{2}{3}\,\dot{\boldsymbol{\varepsilon}}^p : \dot{\boldsymbol{\varepsilon}}^p}$ is the macroscopic effective equivalent plastic strain rate. The evolution of the equivalent plastic strains in the phases are written in terms of the strain concentration factors $\alpha^{(i)}$ defined in (40) in terms of the optimal values $\hat{y}^{(r)}\left(\mathbf{q}_{n+1}\right)$, i.e.,

$$\dot{q}_i = \dot{\bar{\varepsilon}}\,\alpha^{(i)}(\mathbf{q}_{n+1}), \qquad\qquad i = 1, 2, \cdots, N. \tag{66}$$

5.1 Numerical integration of constitutive equations

In the following, we present a method for the numerical integration of the resulting constitutive equations in the context of a displacement driven finite element formulation. In a finite element environment, the solution is developed incrementally and the constitutive equations are integrated at the element Gauss points. At a Gauss point in the finite element mesh, the solution $(\boldsymbol{\varepsilon}_n, \boldsymbol{\sigma}_n, \mathbf{q}_n)$ at time t_n as well as the infinitesimal strain $\boldsymbol{\varepsilon}_{n+1}$ at time t_{n+1} are known, and the problem is to determine $(\boldsymbol{\sigma}_{n+1}, \mathbf{q}_{n+1})$.
A *backward Euler* integration scheme is used for the numerical integration of the flow rule (65):

$$\Delta\boldsymbol{\varepsilon}^p = \Delta\bar{\varepsilon}\,\mathbf{N}_{n+1}. \tag{67}$$

The elasticity equation (60) is written in the form

$$\boldsymbol{\sigma}_{n+1} = \boldsymbol{\sigma}_n + \boldsymbol{\mathcal{L}}^e : (\Delta\boldsymbol{\varepsilon} - \Delta\boldsymbol{\varepsilon}^p) = \boldsymbol{\sigma}^e - 2\,\mu\,\Delta\bar{\varepsilon}\,\mathbf{N}_{n+1}, \tag{68}$$

where $\boldsymbol{\sigma}^e = \boldsymbol{\sigma}_n + \boldsymbol{\mathcal{L}}^e : \Delta\boldsymbol{\varepsilon}$ is the (known) "elastic predictor". Considering the deviatoric part of last equation and using the definition (65) of $\mathbf{N}_{n+1}$ we conclude that the stress deviator $\mathbf{s}_{n+1}$ is co-linear with the deviatoric part of the elastic predictor $\mathbf{s}^e$. Therefore, we can determine the direction $\mathbf{N}_{n+1}$ of the plastic strain rate at t_{n+1} by using the known elastic predictor as

$$\mathbf{N}_{n+1} = \frac{3}{2\,\sigma_e}\,\mathbf{s}_{n+1} = \frac{3}{2\,\sigma_e^e}\,\mathbf{s}^e = \text{known}, \tag{69}$$

where $\sigma_e^e = \sqrt{\frac{3}{2}\,\mathbf{s}^e : \mathbf{s}^e}$ is the von Mises equivalent stress of the elastic predictor. Projecting (68) in the direction of the plastic strain rate $\mathbf{N}_{n+1}$ and taking into account that $\boldsymbol{\sigma} : \mathbf{N} = \sigma_e$ and $\mathbf{N} : \mathbf{N} = \frac{3}{2}$, we find $\sigma_e|_{n+1} = \sigma_e^e - 3\,\mu\,\Delta\bar{\varepsilon}$. Therefore, the yield condition (64) can be written at the end of the increment in the form

$$\sigma_e^e - 3\,\mu\,\Delta\bar{\varepsilon} - \tilde{\sigma}_0\,(\mathbf{q}_n + \Delta\mathbf{q}) = 0. \tag{70}$$

The evolution of the equivalent plastic strains in the phases (66) are written also as

$$\Delta q_i = \Delta\bar{\varepsilon}\,\alpha^{(i)}(\mathbf{q}_n + \Delta\mathbf{q}), \qquad\qquad i = 1, 2, \cdots, N. \tag{71}$$

The problem of integrating the elastoplastic equations for the homogenized composite reduces to the solution of the set of $N+1$ non-linear equations (70) and (71) for $\Delta\bar{\varepsilon}$ and $\Delta\mathbf{q} = \left(\Delta\bar{\varepsilon}^{(1)}, \Delta\bar{\varepsilon}^{(2)}, \cdots, \Delta\bar{\varepsilon}^{(N)}\right)$. These equations are solved by using Newton's method. In every Newton iteration the values of $\Delta\mathbf{q}$ are used to calculate the corresponding $\sigma_0^{(i)}$ from (62) and then the optimization problem (39) is solved by using the CONMAX software [18] to determine the optimal values $\hat{y}^{(i)}$; the values of the effective flow stress $\tilde{\sigma}_0$ and the strain concentration factors $\alpha^{(i)}$ are then determined and the iterations are continued until the set tolerances are met. Details on the calculation of the Jacobian of the Newton loop are given in [27].
It is emphasized that the calculations are much simpler for a two-phase composite; in that case, one does not need to invoke CONMAX, since $\tilde{\sigma}_0$ is defined analytically by (45).
Once $\Delta\bar{\varepsilon}$ and $\Delta\mathbf{q}$ are calculated, equations (68) and (71) are used to determine the stress $\boldsymbol{\sigma}_{n+1}$ and the state variables $\mathbf{q}_{n+1}$.

Remark 1. In the special case where the value $\beta = 0$ is used in (62), the effective flow stress of the composite $\tilde{\sigma}_0$ and the strain concentration factors $\alpha^{(i)}$ are determined using the values of the flow stresses of the phases $\sigma_0^{(i)}\Big|_n$ at the start of the increment, and equations (70) and (71) can be solved analytically:

$$\Delta\bar{\varepsilon} = \frac{\sigma_e^e - \tilde{\sigma}_0\left(\mathbf{q}_n\right)}{3\,\mu} \qquad \text{and} \qquad \Delta q_i = \Delta\bar{\varepsilon}\,\alpha^{(i)}(\mathbf{q}_n). \tag{72}$$

The integration scheme described above is implemented into the ABAQUS general purpose finite element program [13]. This code provides a general interface so that a particular constitutive model can be introduced as a user subroutine (UMAT). The finite element formulation is based on the weak form of the momentum balance, the solution is carried out incrementally, and the discretized nonlinear equations are solved using Newton's method. In the calculations, the Jacobian of the global Newton scheme is approximated by the tangent stiffness matrix. Such an approximation of the Jacobian is first-order accurate as the size of the increment $\Delta t \to 0$; it should be emphasized, however, that the aforementioned approximation influences only the rate of convergence of the Newton loop and not the accuracy of the results.

5.2 Unit cell calculations and assessment of the model with hardening phases

In this section we present the results of unit cell finite element calculations for a composite material made up of a statistically isotropic random distribution of isotropic, linearly-elastic hardening-plastic spherical inclusions embedded in a continuous, isotropic, linearly-elastic hardening-plastic matrix. All analyses were carried out incrementally and accounted for geometry changes due to deformation (finite strain solutions).

In all cases analyzed, the matrix material is identified as "phase 1" and the flow stress $\sigma_y^{(i)}$ of "phase i" is a function of the corresponding equivalent plastic strain $\bar{\varepsilon}^p$:

$$\sigma_y^{(i)}\left(\bar{\varepsilon}^{(i)}\right) = \sigma_0^{(i)}\left(1 + \frac{\bar{\varepsilon}^{(i)}}{\varepsilon_0^{(i)}}\right)^{\frac{1}{\eta^{(i)}}}, \qquad \varepsilon_0^{(i)} = \frac{\sigma_0^{(i)}}{E}, \tag{73}$$

where $\sigma_0^{(i)} = \sigma_y^{(i)}(0)$ is the yield stress of phase i, E is the elastic Young's modulus, and the hardening exponents $\eta^{(i)}$ take values in the region $1 \le \eta^{(i)} \le \infty$, with the limiting case $\eta^{(i)} = \infty$ corresponding to perfect plasticity. Note that this hardening exponents are completely uncorrelated to the creep exponent $n^{(i)}$ used in the definitions of the stress potentials in the previous sections.

The values $E = 917\,\sigma_0^{(1)}$ and $\nu = 0.3$ for Young's modulus E and Poisson ratio ν are used in the calculations. In addition, one-element finite element calculations were carried out, in which the element is subjected to the same deformation gradient as the unit cell and the corresponding uniform stress state in the element is calculated by using the algorithm described in section 5.1 for the homogenized material.

5.2.1 Two-phase composites

We analyze first a two-phase composite with

$$\frac{\sigma_0^{(2)}}{\sigma_0^{(1)}} = 1.5, \qquad \eta^{(1)} = 5, \qquad \eta^{(2)} = 3. \tag{74}$$

The corresponding stress-strain curves of the phases in uniaxial tension are shown in Fig. 10.

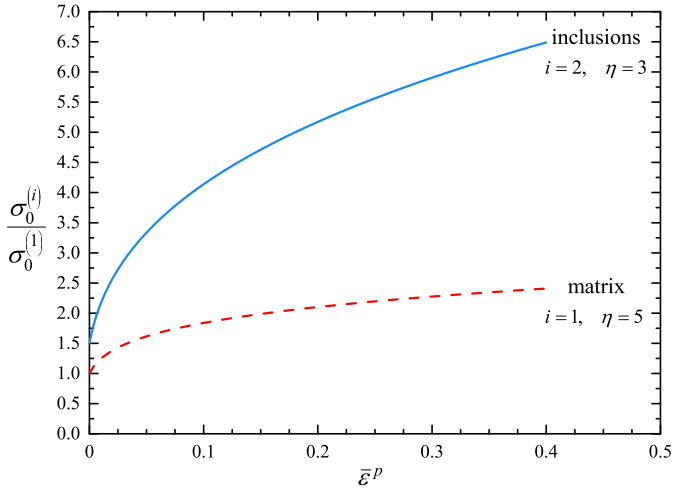

Figure 10: Uniaxial stress-strain curves of phases.

Figure 11 shows the results of the unit cell finite element calculations together with the predictions of the homogenization model for the case of uniaxial tension in direction 1 and for inclusion volume fractions c_2 =0.10, 0.20, 0.30, and 0.40. The quantity $\tilde{\sigma}$ in Fig. 11 is the average stress $< \sigma_{11} >$ in the unit cell calculations and the uniform σ_{11} stress component in the corresponding one-element homogenization calculation. The predictions of the homogenization model agree well with the numerical results. It is also evident from these figures that as we increase the volume fraction of the stiffer particle phase which also has a higher hardening exponent, this leads to a reinforcement of the composite both at the level of the yield strength as well as in its hardening response. It is also interesting to note that even though we have added the hardening behavior of the phases heuristically to the homogenization model for perfectly plastic phases (see equation (45)), the corresponding analytical estimates are in excellent agreement with those obtained by the finite element calculations (see also relevant discussion in [44]). This, in turn, suggests that such a simplified approach is sufficient for this class of materials.

Calculations are also carried out for finite shear deformation. In this case, the deformation gradient used in (48) is of the form

$$\mathbf{F} = \boldsymbol{\delta} + \gamma\, \mathbf{e}_1\, \mathbf{e}_2, \tag{75}$$

where γ is the amount of shearing on the 1-2 plane. Figure 12 shows the deformed unit cell at $\gamma = 0.15$ for various inclusion volume fractions c_2.

Figure 13 shows the results of the unit cell finite element calculations together with the predictions of the homogenization model for the case of finite shear on the 1-2 plane and for

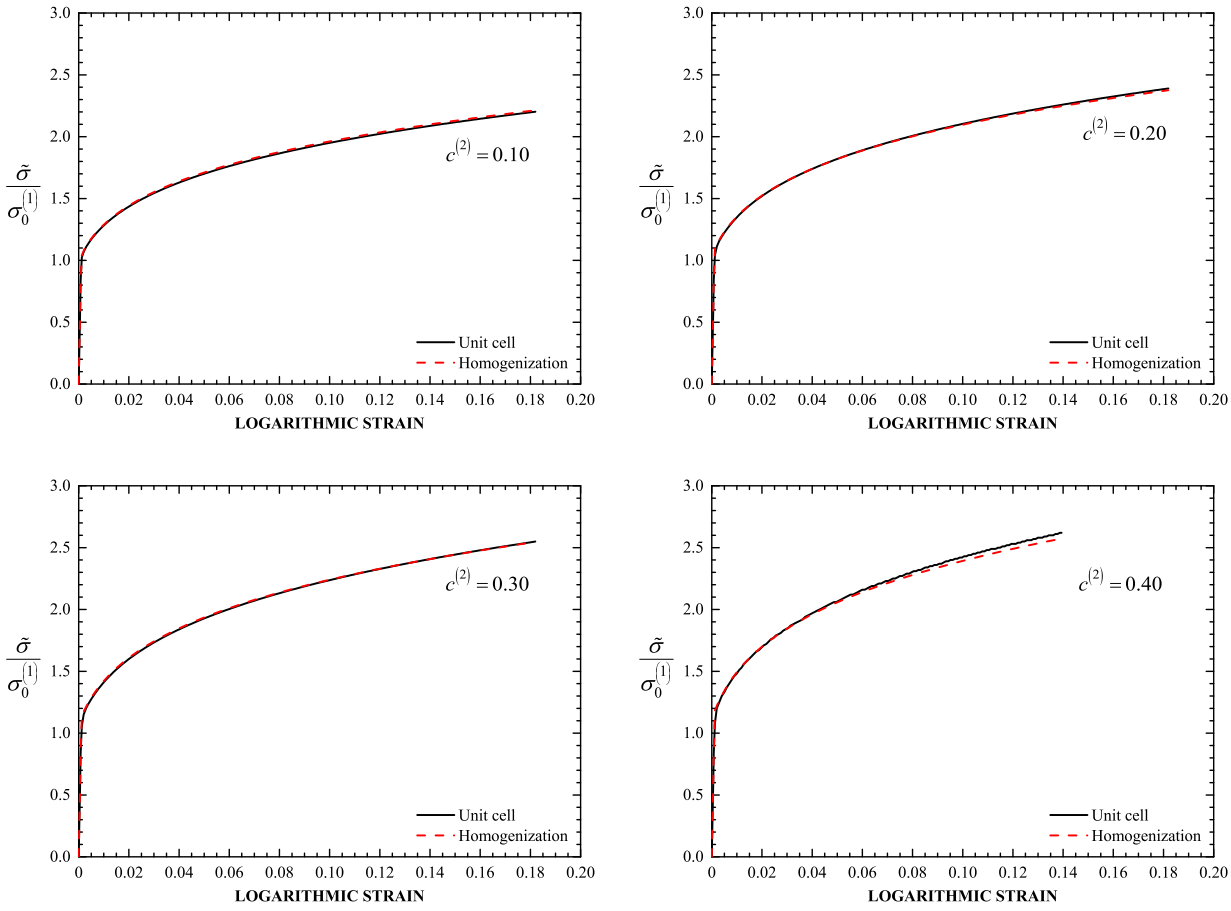

Figure 11: Stress-strain curves of the two-phase composite in uniaxial tension for different values of the volume fraction $c^{(2)}$. The solid lines are the results of the unit cell finite element calculations and the dash lines are the predictions (39) of the model based on the H-S$^-$ estimate ($\mu_0 = \mu^{(1)}$).

inclusion volume fractions c_2 =0.10, 0.20, 0.30, and 0.40. The quantity $\tilde{\tau}$ in Fig. 13 is

$$\tilde{\tau} = \sqrt{\frac{1}{2}\, s_{ij}\, s_{ij}}\,, \tag{76}$$

where s_{ij} is identified with the average deviatoric stresses $< s_{ij} >$ in the unit cell calculations and with the uniform deviatoric stresses s_{ij} in the one-element homogenization calculations. Again, the predictions of the homogenization model agree well with the numerical results. Similar observations to those made in the context of Figure 11 could also be made in Figure 13 regarding the effect of volume fraction and the hardening exponent of the phases upon the effective response under shear loadings.

5.2.2 Three-phase composites

We consider next a three-phase composite with

$$\frac{\sigma_0^{(2)}}{\sigma_0^{(1)}} = 1.875, \quad \frac{\sigma_0^{(3)}}{\sigma_0^{(1)}} = 5, \qquad \eta^{(1)} = 5, \quad \eta^{(2)} = 3, \quad \eta^{(3)} = 2.5. \tag{77}$$

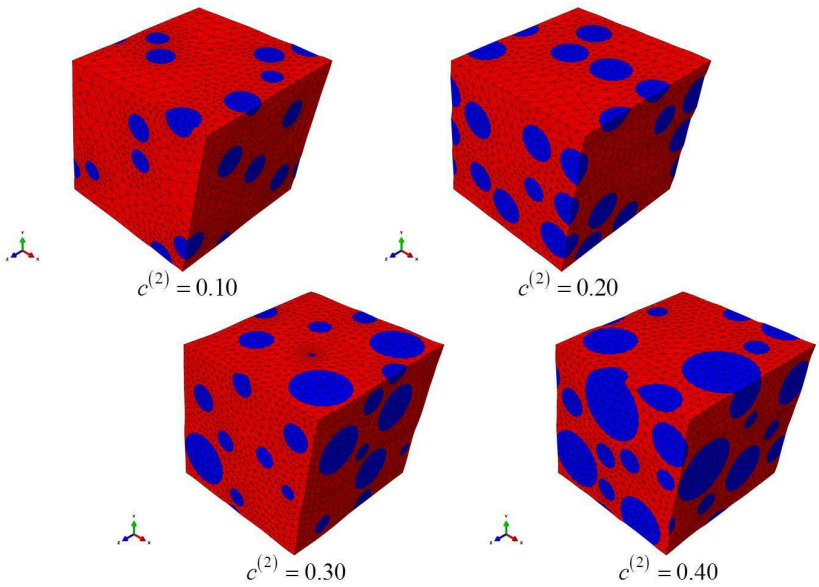

Figure 12: Deformed configurations of unit cells in simple shear ($\gamma = 0.15$) for various values of the volume fraction $c^{(2)}$.

The problems of uniaxial tension and finite shear deformation are solved.
Figure 14 shows the deformed unit cells for uniaxial tension at $\lambda = 1.20$ and finite shear $\gamma = 0.20$.
Figure 15 shows the stress-strain curves in uniaxial tension and finite shear, for a three-phase composite with composition $c^{(1)} = 0.60$, $c^{(2)} = 0.25$, and $c^{(3)} = 0.15$. The predictions of the homogenization model agree well with the results of the unit cell finite element calculations. The model is capable of predicting sufficiently well both the initial yield strength of the three-phase composite as well the hardening evolution as a function of the applied strains both in uniaxial tension and shear loadings.

6 Concluding remarks

The present work presents a simple semi-analytical model for the estimation of the effective as well as the phase average response of $N-$phase incompressible isotropic elasto-plastic metallic materials. The model is based on the original variational method of Ponte Castañeda [29], which is based on a linear comparison composite technique. The resulting expression for the effective yield strength of the composite requires the solution of a constrained optimization problem for $N-1$ scalar variables and is much simpler and tractable than the original expressions given in [30]. This is achieved by use of the methodology of Kaufman *et al.* [18]. In the special case of a two-phase composite, we provide a fully explicit expression which is given via a piecewise function defined in equation (45). Due to its simplicity and numerical efficiency, the proposed $N-$phase model is numerically implemented in a user-material subroutine which, in turn, allows for the simulation of three dimensional geometries.
In addition, the $N-$phase analytical model is compared with full field three dimensional finite element simulations of two- and three-phase multi-particle periodic unit cells. The proposed model is found to be in good agreement with the finite element results in most of the cases considered here, even at large particle volume fractions and different hardening

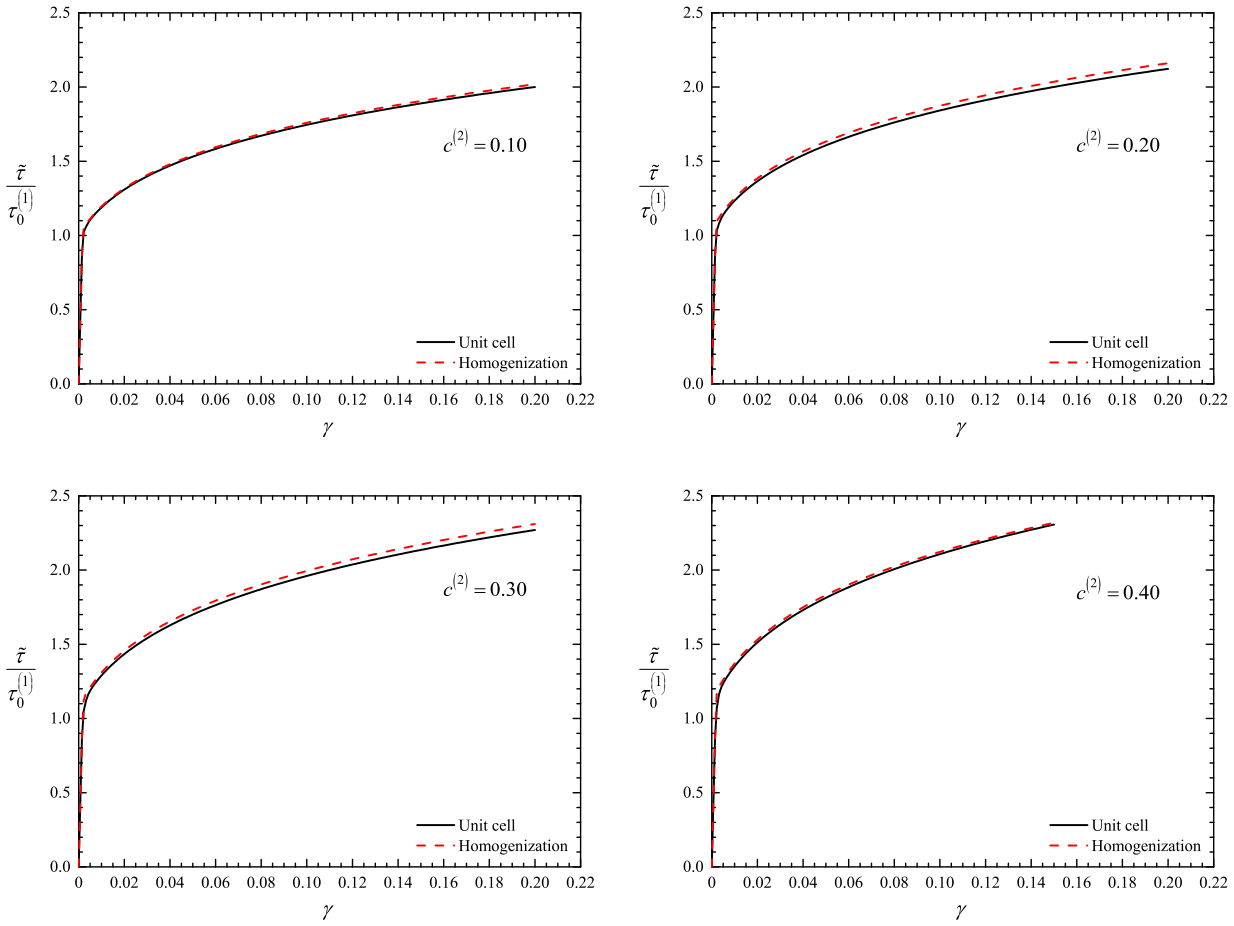

Figure 13: Shear stress-shear strain curves of the two-phase composite in simple shear for different values of the volume fraction $c^{(2)}$. The solid lines are the results of the unit cell finite element calculations and the dash lines are the predictions (39) of the model based on the H-S$^-$ estimate ($\mu_0 = \mu^{(1)}$).

exponents. The agreement is good both for the effective average stress strain response, as well as for the phase average strain fields. This last observation allowed to extend the model in a heuristic manner to account for arbitrary isotropic hardening of the phases, both in a small and finite strain formalism. The present combined analytical and numerical study reveals several nontrivial features which are summarized in the following.

One of the main non-intuitive observations in the present work, which is in accord with former literature, is that in the context of a two-phase composite when the strength of the particles is almost twice that of the matrix the particles behave as being rigid for all volume fractions considered here. In other words, we obtain a rather sharp transition when the yield stress of the particle is about two times that of the matrix beyond which the strain in the particle is negligible, thus leading to an almost rigid response of the particle in the sense of straining for a large range of volume fractions. This result was shown for the effective yield stress by Suquet [44] and Idiart [16] for given particle volume fraction, whereby it is further shown here that this sharp transition is weakly sensitive to the particle volume fraction (at least for volume fractions up to 40%). This, in turn, may have significant implications in the strengthening of the composite and possible debonding/failure of the particle/matrix

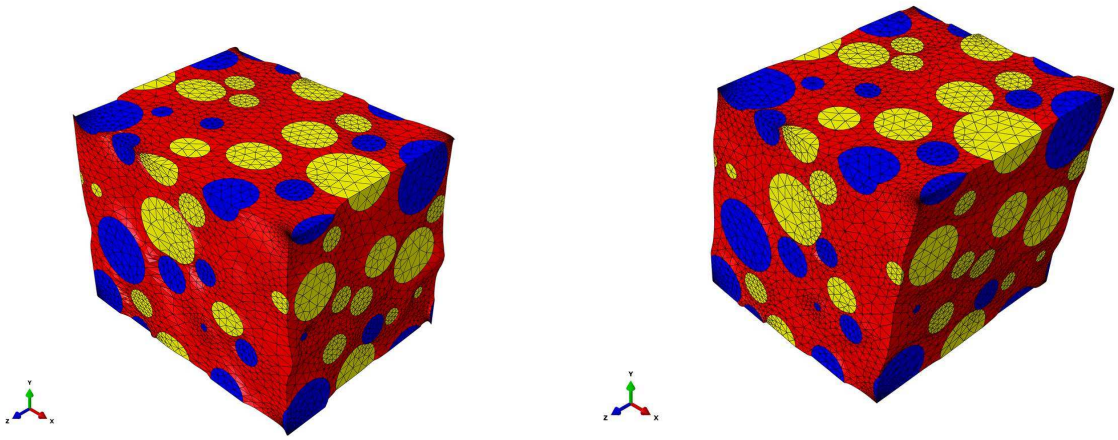

Figure 14: Deformed configurations of unit cells of the three-phase composite in uniaxial tension ($\lambda = 1.20$) and simple shear ($\gamma = 0.20$).

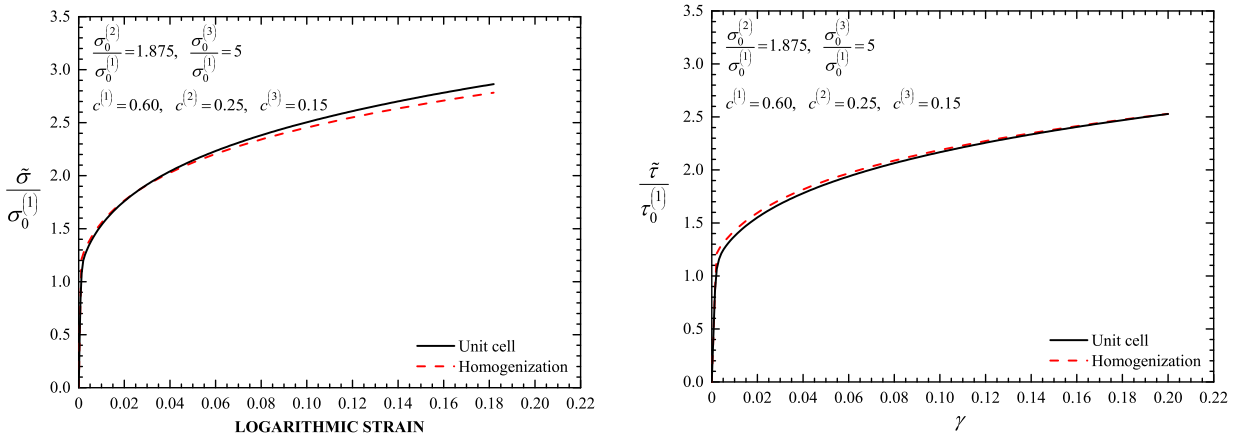

Figure 15: Stress-strain curves of the three-phase composite in uniaxial tension and simple shear. The solid lines are the results of the unit cell finite element calculations and the dash lines are the predictions (39) of the model based on the H-S$^-$ estimate ($\mu_0 = \mu^{(1)}$).

interface [4], since beyond that contrast ratio the particle stops deforming. This of course leads to stress and strain concentrations in the matrix/article interface.

A second observation, which has already been made in the context of a plastic matrix with rigid particles by Suquet [44] and Idiart [16] is that the numerical estimates exhibit a dependence on the third invariant (J_3) of the stress tensor, i.e., on the Lode parameter or Lode angle. Nonetheless, this dependence is extremely weak and thus the present model, which does not take into account this dependence, is sufficiently accurate for the estimation of the effective response as well as of the phase average strains (which depend apriori upon the normal to the yield surface). This observation of course is valid for phases described by a von Mises (J_2) yield response and does not hold in the case of plastic solids that depend directly on the third invariant J_3 via Tresca, Hoshford or Drucker-Prager plasticity (see for instance Barthélémy and Dormieux [1] and Barthélémy *et al.* [22]).

A third, and perhaps more important finding of this work at least from a more practical point of view, is related to the extension of the model to arbitrary isotropic hardening of the

phases. In the present work, we carry out first the nonlinear homogenization for perfectly plastic phases and then the hardening is added heuristically at the definition of the yield stresses of each of the phases. This of course is an approximation and does not take into account explicitly the coupling between the different hardening exponents of the different phases. Nevertheless, the resulting estimates are in very good agreement with the full field finite element results (which include this coupling) suggesting that this strategy is sufficient for the materials and loadings considered in this study. This good agreement can be directly associated with the fact that the model predicts accurately enough the phase average strains. This, however, may not be true if one considers kinematic hardening of the phases or more complex non-proportional loadings but again in this case a more advanced homogenization method needs to be used such as the one proposed by Lahellec and Suquet [19].
Finally, in this study, we do not consider the extreme case of a three-phase composite comprising stiff particles and voids. The reason is that the presence of a soft compressible phase would introduce a dependence on an additional invariant, i.e, pressure (I_1) and the material would be plastically compressible (see for instance Garajeu and Suqet [11] and He *et al.* [12]). A vast amount of studies has been carried out in the context of voided materials and is very well known that the present method by default would lead to overly stiff estimates unless corrected (see for instance recent work of Danas and Aravas [7] and Cao *et al.* [6]). Such work is now underway and will be reported elsewhere.

Acknowledgments

This work was carried out while I.P. and N.A. were supported by the Greek General Secretariat for Research and Technology (GSRT) through the ΚΡΗΠΙΣ Project. K.D. greatfully acknowledge partial support by the French National Research Agency (ANR) via the grant INDiANA (ANR-12-RMNP-0011). The authors would like also to acknowledge the help of late Prof. A. Stamatis of University of Thessaly on the solution of the optimization problem. Use of the FORTRAN code CONMAX (`http://www.netlib.org/opt/conmax.f`) is gratefully acknowledged.

Appendix: Finite strain formulation

The constitutive equations become

$$\mathbf{D} = \mathbf{D}^e + \mathbf{D}^p, \tag{78}$$

$$\mathbf{D}^e = \boldsymbol{\mathcal{M}}^e : \overset{\nabla}{\boldsymbol{\sigma}}, \tag{79}$$

$$\mathbf{D}^p = \dot{\bar{\varepsilon}}\,\mathbf{N}, \qquad \mathbf{N} = \frac{3}{2\,\sigma_e}\,\mathbf{s}, \tag{80}$$

$$\sigma_0^{(i)} = (1-\beta)\;\sigma_0^{(i)}\Big|_n + \beta\;\sigma_0^{(i)}\Big|_{n+1}, \tag{81}$$

$$\Phi(\boldsymbol{\sigma}, \mathbf{q}) = \sigma_e - \tilde{\sigma}_0(\mathbf{q}) = 0, \tag{82}$$

$$\dot{q}_i = \dot{\bar{\varepsilon}}\,\alpha^{(i)}(\mathbf{q}), \qquad i = 1, 2, \cdots, N, \tag{83}$$

where ∇ denotes the Jaumann or co-rotational derivative.
In a finite element environment, the solution is developed incrementally and the constitutive equations are integrated at the element Gauss integration points. Let $\mathbf{F}$ denote the deformation gradient tensor. At a given Gauss point, the solution $(\mathbf{F}_n, \boldsymbol{\sigma}_n, \mathbf{q}_n)$ at time t_n as well as the deformation gradient $\mathbf{F}_{n+1}$ at time t_{n+1} are known, and the problem is to determine $(\boldsymbol{\sigma}_{n+1}, \mathbf{q}_{n+1})$.
The time variation of the deformation gradient $\mathbf{F}$ during the time increment $[t_n, t_{n+1}]$ can be written as

$$\mathbf{F}(t) = \Delta\mathbf{F}(t) \cdot \mathbf{F}_n = \mathbf{R}(t) \cdot \mathbf{U}(t) \cdot \mathbf{F}_n, \qquad t_n \le t \le t_{n+1}, \tag{84}$$

where $\mathbf{R}(t)$ and $\mathbf{U}(t)$ are the rotation and right stretch tensors associated with $\Delta\mathbf{F}(t)$. The corresponding deformation rate $\mathbf{D}(t)$ and spin $\mathbf{W}(t)$ tensors are given by

$$\mathbf{D}(t) \equiv \left[\dot{\mathbf{F}}(t) \cdot \mathbf{F}^{-1}(t)\right]_s = \left[\Delta\dot{\mathbf{F}}(t) \cdot \Delta\mathbf{F}^{-1}(t)\right]_s, \tag{85}$$

and

$$\mathbf{W}(t) \equiv \left[\dot{\mathbf{F}}(t) \cdot \mathbf{F}^{-1}(t)\right]_a = \left[\Delta\dot{\mathbf{F}}(t) \cdot \Delta\mathbf{F}^{-1}(t)\right]_a, \tag{86}$$

where the subscripts s and a denote the symmetric and anti-symmetric parts, respectively.
If it is assumed that the Lagrangian triad associated with $\Delta\mathbf{F}(t)$ (i.e., the eigenvectors of $\mathbf{U}(t)$) remains fixed over the time interval (t_n, t_{n+1}), it can be shown readily that

$$\mathbf{D}(t) = \mathbf{R}(t) \cdot \dot{\mathbf{E}}(t) \cdot \mathbf{R}^T(t), \quad \mathbf{W}(t) = \dot{\mathbf{R}}(t) \cdot \mathbf{R}^T(t), \quad \overset{\nabla}{\boldsymbol{\sigma}}(t) = \mathbf{R}(t) \cdot \dot{\hat{\boldsymbol{\sigma}}}(t) \cdot \mathbf{R}^T(t), \tag{87}$$

where a superscript T indicates the transpose of a second-order tensor, $\mathbf{E}(t) = \ln \mathbf{U}(t)$ is the logarithmic strain relative to the configuration at the start of the increment, and $\hat{\boldsymbol{\sigma}}(t) = \mathbf{R}^T(t) \cdot \boldsymbol{\sigma}(t) \cdot \mathbf{R}(t)$.
It is noted that at the start of the increment $(t = t_n)$

$$\Delta\mathbf{F}_n = \mathbf{R}_n = \mathbf{U}_n = \boldsymbol{\delta}, \qquad \hat{\boldsymbol{\sigma}}_n = \boldsymbol{\sigma}_n, \quad \text{and} \qquad \mathbf{E}_n = \mathbf{0}, \tag{88}$$

whereas at the end of the increment $(t = t_{n+1})$

$$\Delta\mathbf{F}_{n+1} = \mathbf{F}_{n+1} \cdot \mathbf{F}_n^{-1} = \mathbf{R}_{n+1} \cdot \mathbf{U}_{n+1} = \text{known}, \quad \text{and} \quad \mathbf{E}_{n+1} = \ln \mathbf{U}_{n+1} = \text{known}. \tag{89}$$

Then, the constitutive equations of the model can be written as

$$\dot{\mathbf{E}} = \dot{\mathbf{E}}^e + \dot{\mathbf{E}}^p \qquad \text{or} \qquad \mathbf{E} = \mathbf{E}^e + \mathbf{E}^p, \tag{90}$$

$$\dot{\mathbf{E}}^e = \boldsymbol{\mathcal{M}}^e : \dot{\hat{\boldsymbol{\sigma}}} \qquad \text{or} \qquad \mathbf{E}^e_{n+1} = \boldsymbol{\mathcal{M}}^e : (\hat{\boldsymbol{\sigma}}_{n+1} - \boldsymbol{\sigma}_n)\,, \tag{91}$$

$$\dot{\mathbf{E}}^p = \dot{\bar{\varepsilon}}\,\hat{\mathbf{N}}, \qquad \hat{\mathbf{N}} = \frac{3}{2\,\sigma_e}\,\hat{\mathbf{s}}, \tag{92}$$

$$\sigma_0^{(i)} = (1-\beta)\;\sigma_0^{(i)}\Big|_n + \beta\;\sigma_0^{(i)}\Big|_{n+1}\,, \tag{93}$$

$$\Phi(\hat{\boldsymbol{\sigma}}, \mathbf{q}) = \sigma_e - \tilde{\sigma}_0(\mathbf{q}) = 0, \tag{94}$$

$$\dot{q}_i = \dot{\bar{\varepsilon}}\,\alpha^{(i)}(\mathbf{q}), \qquad i = 1, 2, \cdots, N, \tag{95}$$

where we took into account that $\mathbf{E}^e_n = \mathbf{0}$, $\hat{\boldsymbol{\sigma}}_n = \boldsymbol{\sigma}_n$, and $\sigma_e = \sqrt{\frac{3}{2}\,\mathbf{s} : \mathbf{s}} = \sqrt{\frac{3}{2}\,\hat{\mathbf{s}} : \hat{\mathbf{s}}}$. The constitutive equations listed above are identical to those of the infinitesimal strain formulation and can be integrated as described in section 5. The integration determines $\hat{\boldsymbol{\sigma}}_{n+1}$ and the true stresses are calculated as $\boldsymbol{\sigma}_{n+1} = \mathbf{R}_{n+1} \cdot \hat{\boldsymbol{\sigma}}_{n+1} \cdot \mathbf{R}^T_{n+1}$.

References

[1] J.F. Barthélémy and L. Dormieux, 'A micromechanical approach to the strength criterion of drucker-prager materials reinforced by rigid inclusions', *Int. J. Numer. Anal. Methods Geomech.* **28** (2004), 565–582.

[2] I. Barsoum and J. Faleskog, 'Rupture mechanisms in combined tension and shear — Micromechanics', *Int. J. Solids Struct.* **44** (2007) 5481–5498.

[3] D. Bonnenfant, F. Mazerolle and P. Suquet, 'Compaction of powders containing hard inclusions: experiments and micromechanical modeling', *Mechanics of Materials* **29** (1998) 93–109.

[4] F. Bignonnet, L. Dormieux and E. Lemarchand, 'Strength of a matrix with elliptic criterion reinforced by rigid inclusions with imperfect interfaces', *European Journal of Mechanics A/Solids* **52** (2015) 95–106.

[5] L. Brassart, L. Stainier, I. Doghri and L. Delannay, 'A variational formulation for the incremental homogenization of elasto-plastic composites', *J. Mech. Phys. Solids*, **59** (2011) 2455–2475.

[6] T.-S. Cao, M. Maziere, K. Danas and J. Besson, 'A model for ductile damage prediction at low stress triaxialities incorporating void shape change and void rotation', *Int. J. Solids Struct.* **63** (2015), 240-263.

[7] K. Danas and N. Aravas, 'Numerical modeling of elasto-plastic porous materials with void shape effects at finite deformations', *Composites: Part B* **43** (2012), 2544–2559.

[8] G. deBotton and P. Ponte Castañeda, 'Elastoplastic constitutive relations for fiber-reinforced solids', *Int. J. Solids Struct.* **30** (1993) 1865–1890.

[9] J.D. Eshelby, 'The determination of the elastic field of an ellipsoidal inclusion, and related problems', *Proc. R. Soc. Lond. A* **241** (1957) 376–396.

[10] F. Fritzen, S. Forest, T. Böhlke, D. Kondo and T. Kanit, 'Computational homogenization of elasto-plastic porous metals', *Int. J. Plast.* **29**, 102–119.

[11] M. Gărăjeu and P. Suquet, 'Effective properties of porous ideally plastic or viscoplastic materials containing rigid particles', *J. Mech. Phys. Solids* **45** (1997), 873–902.

[12] Z. He, L. Dormieux and D. Kondo, 'Strength properties of a DruckerPrager porous medium reinforced by rigid particles', *Int. J. Plasticity* **51** (2013) 218–240.

[13] H.D. Hibbitt, 'ABAQUS/EPGEN — A general purpose finite element code with emphasis in nonlinear applications', *Nucl. Engng. Des.* **77** (1977) 271–297.

[14] R. Hill, 'A self-consistent mechanics of composite materials', *J. Mech. Phys. Solids* **13** (1965) 213–222.

[15] M.I. Idiart, H. Moulinec, P. Ponte Castañeda and P. Suquet, 'Macroscopic behavior and field fluctuations in viscoplastic composites: Second-order estimates versus full-field-simulations', *J. Mech. Phys. Solids* **54** (2006) 1029–1063.

[16] M. Idiart, 'Modeling the macroscopic behavior of two-phase nonlinear composites by infinite rank laminates', *J. Mech. Phys. Solids* **56** (2008) 2599–2617.

[17] M. Kailasam and P. Ponte Castañeda, 'A general constitutive theory for linear and nonlinear particulate media with microstructure evolution', *J. Mech. Phys. Solids* **46** (1998) 427–465.

[18] E.H. Kaufman, Jr., D.J. Leeming and G.D. Taylor, 'An ODE-based approach to nonlinearly constrained minimax problems', *Numerical Algorithms* **9** (1995) 25–37 (CONMAX software available at `http://www.netlib.org/cgi-bin/search.pl`).

[19] N. Lahellec and P. Suquet, 'On the effective behavior of nonlinear inelastic composites: I. Incremental variational principles', *J. Mech. Phys. Solids* **55** (2007a) 1932–1963.

[20] N. Lahellec and P. Suquet, 'On the effective behavior of nonlinear inelastic composites: II. A second-order procedure', *J. Mech. Phys. Solids* **55**, (2007b) 1964–1992.

[21] O. Lopez-Pamies, T. Goudarzi and K. Danas, 'The nonlinear elastic response of suspensions of rigid inclusions in rubber. II. A simple explicit approximation for finite-concentration suspensions', *J. Mech. Phys. Solids* **61** (2013) 19–37.

[22] S. Maghous, L. Dormieux and J.F. Barthélémy, 'Micromechanical approach to the strength properties of frictional geomaterials', *Eur. J. Mech. A/Solids* 28 (2009), 179–188.

[23] A. Mbiakop, A. Constantinescu and K. Danas, 'On void shape effects of periodic elasto-plastic materials subjected to cyclic loading', *Eur. J. Mech. A/Solids* **49** (2015) 481–499.

[24] A. Mbiakop, A. Constantinescu and K. Danas, 'An analytical model for porous single crystals with ellipsoidal voids', *J. Mech. Phys. Solids* **84** (2015) 436–467.

[25] J.C. Michel and P. Suquet, 'The constitutive law of nonlinear viscous and porous materials', *J. Mech. Phys. Solids* **40** (1992) 783–812

[26] J.C. Michel, H. Moulinec and P. Suquet, 'Effective properties of composite materials with periodic microstructure: a computational approach', *Comp. Methods Appl. Mech. Eng.* **172** (1999) 109–143.

[27] I. Papadioti, 'Non-linear homogenization theories', Ph.D. Thesis, University of Thessaly, Greece, in preparation.

[28] I. Papatriantafillou, M. Agoras, N. Aravas and G. Haidemenopoulos, 'Constitutive modeling and finite element methods for TRIP steels', *Comp. Methods Appl. Mech. Eng.* **195** (2006) 5094–5114.

[29] P. Ponte Castañeda, 'The effective mechanical properties of nonlinear isotropic composites', *J. Mech. Phys. Solids* **39** (1991) 45–71.

[30] P. Ponte Castañeda, 'New variational principles in plasticity and their application to composite materials', *J. Mech. Phys. Solids* **40** (1992) 1757–1788.

[31] P. Ponte Castañeda, 'Nonlinear composite materials: Effective constitutive behavior and microstructure evolution', in *Continuum Micromechanics*, CISM Courses and Lectures No. 377 (ed. P. Suquet), Springer-Verlag (1997) 131–195.

[32] P. Ponte Castañeda, 'Second-order homogenization estimates for nonlinear composites incorporating field fluctuations: I–theory', *J. Mech. Phys. Solids* **50** (2002) 737–757.

[33] P. Ponte Castañeda and P. Suquet, 'Nonlinear composites', *Advances in Applied Mechanics* **34** (1998) 171–302.

[34] P. Ponte Castañeda, 'Heterogeneous Materials', *Lecture Notes*, École Polytechnique, Department of Mechanics, ISBN 2-7302-1267-1 (2005).

[35] P. Ponte Castañeda and P. Suquet, 'On the effective mechanical behavior of weakly inhomogeneous nonlinear materials', *Eur. J. Mech. A/Solids* **14** (1995) 205–236.

[36] P. Ponte Castañeda and P. Suquet, 'Nonlinear Composites and Microstructure evolution', in H. Aref and J. Phillips (eds.) Mechanics for a new Millenium, Kluwer Acad. Pub. (2001) 253–273.

[37] P. Ponte Castañeda and M. Zaidman, 'Constitutive models for porous materials with evolving microstructure', *J. Mech. Phys. Solids* **42** (1994) 1459–1497.

[38] M.D. Rintoul and S. Torquato, 'Reconstruction of the structure of despersions', *J. Collois Inter. Sci.* **186** (1997) 467–476.

[39] J. Segurado and J. Llorca, 'A numerical approximation to the elastic properties of sphere-reinforced composites', *J. Mech. Phys. Solids* **50** (2002) 2107–2121.

[40] J. Schöberl, NETGEN An advancing front 2D/3D-mesh generator based on abstract rules *Computing and Visualization in Science* **1** (1997) 41–52.

[41] P. Suquet, 'Elements of homogenization for inelastic solids', in *Homogenization Techniques for Composite Media* (eds. E. Sanchez-Palencias and A. Zaoui), Springer-Verlag (1987) 194–278.

[42] P. Suquet and P. Ponte Castañeda, 'Small-contrast perturbation expansions for the effective properties of nonlinear composites', *C. R. Acad. Sci. Paris (Série II)* **317** (1993) 1515–1522.

[43] P. Suquet, 'Overall properties of nonlinear composites: a modified secant moduli theory and its link with Ponte Castañeda's nonlinear variational procedure', *C. R. Acad. Sci. Paris (Série II)* **320** (1995) 563–71.

[44] P. Suquet, 'Effective properties of nonlinear composites', in *Continuum Micromechanics*, CISM Courses and Lectures No. 377 (ed. P. Suquet), Springer-Verlag (1997) 197–264.

[45] J.R. Wilis, 'Bounds and self-consistent estimates for the overall properties of anisotropic composites', *J. Mech. Phys. Solids* **25** (1977) 185–202.

[46] J.R. Willis, 'Elasticity theory of composites', in *Mechanics of Solids*, The Rodney Hill 60th Anniversary Volume (eds. H.G. Hopkins and M.J. Sewell), Pergamon Press (1982) 653–686.